

Cosmological Results from High- z Supernovae^{1,2}

John L. Tonry,³ Brian P. Schmidt,⁴ Brian Barris,³ Pablo Candia,⁵ Peter Challis,⁶ Alejandro Clocchiatti,⁷ Alison L. Coil,⁸ Alexei V. Filippenko,⁸ Peter Garnavich,⁹ Craig Hogan,¹⁰ Stephen T. Holland,⁹ Saurabh Jha,^{6,8} Robert P. Kirshner,⁶ Kevin Krisciunas,^{5,11} Bruno Leibundgut,¹² Weidong Li,⁸ Thomas Matheson,⁶ Mark M. Phillips,¹¹ Adam G. Riess,¹³ Robert Schommer,^{5,15} R. Chris Smith,⁵ Jesper Sollerman,¹⁴ Jason Spyromilio,¹² Christopher W. Stubbs,¹⁰ and Nicholas B. Suntzeff⁵

ABSTRACT

The High- z Supernova Search Team has discovered and observed 8 new supernovae in the redshift interval $z = 0.3$ – 1.2 . These independent observations, analyzed by similar but distinct methods, confirm the result of Riess et al. (1998a) and Perlmutter et al. (1999) that supernova luminosity distances imply an accelerating universe. More importantly, they extend the redshift range of consistently observed SN Ia to $z \approx 1$, where the signature of cosmological effects has the opposite sign of some plausible systematic effects. Consequently, these measurements not only provide another quantitative confirmation of the importance of dark energy, but also constitute a powerful qualitative test for the cosmological origin of cosmic acceleration. We find a rate for SN Ia of $(1.4 \pm 0.5) \times 10^{-4} h^3 \text{ Mpc}^{-3} \text{ yr}^{-1}$ at a mean redshift of 0.5. We present distances and host extinctions for 230 SN Ia. These place the following constraints on cosmological quantities: if the equation of state parameter of the dark energy is $w = -1$, then $H_0 t_0 = 0.96 \pm 0.04$, and $\Omega_\Lambda - 1.4\Omega_M = 0.35 \pm 0.14$. Including the constraint of a flat Universe, we find $\Omega_M = 0.28 \pm 0.05$, independent of any large-scale structure measurements. Adopting a prior based on the 2dF redshift survey constraint on Ω_M and assuming a flat universe, we find that the equation of state parameter of the dark energy lies in the range $-1.48 < w < -0.72$ at 95% confidence. If we further assume that $w > -1$, we obtain $w < -0.73$ at 95% confidence. These constraints are similar in precision and in value to recent results reported using the WMAP satellite, also in combination with the 2dF redshift survey.

Subject headings: galaxies: distances and redshifts — cosmology: distance scale — supernovae: general

¹Based in part on observations with the NASA/ESA *Hubble Space Telescope*, obtained at the Space Telescope Science Institute, which is operated by the Association of Universities for Research in Astronomy (AURA), Inc., under NASA contract NAS 5-26555. This research is primarily associated with proposal GO-8177, but also uses and reports results from proposals GO-7505, 7588, 8641, and 9118.

²CFHT: Based in part on observations taken with the Canada-France-Hawaii Telescope, operated by the National Research Council of Canada, le Centre National de la Recherche Scientifique de France, and the University of Hawaii. CTIO: Based in part on observations taken at the Cerro Tololo Inter-American Observatory. Keck: Some of the data presented herein were obtained at the W. M. Keck Observatory, which is operated as a scientific partnership

among the California Institute of Technology, the University of California, and the National Aeronautics and Space Administration. The Observatory was made possible by the generous financial support of the W. M. Keck Foundation. UH: Based in part on observations with the University of Hawaii 2.2-m telescope at Mauna Kea Observatory, Institute for Astronomy, University of Hawaii. UKIRT: Based in part on observations with the United Kingdom Infrared Telescope (UKIRT) operated by the Joint Astronomy Centre on behalf of the U.K. Particle Physics and Astronomy Research Council. VLT: Based in part on observations obtained at the European Southern Observatory, Paranal, Chile, under programs ESO 64.O-0391 and ESO 64.O-0404. WIYN: Based in part on observations taken at the WIYN Observatory, a joint facility of the University of Wisconsin-Madison, Indiana University, Yale University,

1. Introduction

1.1. SN Ia and the Accelerating Universe

Discovering Type Ia supernovae (SN Ia) with the intent of measuring the history of cosmic expansion began in the 1980s with pioneering efforts by Nørgaard-Nielsen et al. (1989). Their techniques, extended by the Supernova Cosmology Project (Perlmutter et al. 1995) and by the High- z Supernova Search Team (HZT; Schmidt et al. 1998), started to produce interesting results once large-format CCDs were introduced on fast telescopes. Efforts to improve the use of SN Ia as standard candles by Phillips (1993), Hamuy et al. (1995), and Riess, Press & Kirshner (1996) meant that data from a modest number of these objects

and the National Optical Astronomy Observatories.

³Institute for Astronomy, University of Hawaii, 2680 Woodlawn Drive, Honolulu, HI 96822; jt@ifh.hawaii.edu, barris@ifh.hawaii.edu

⁴The Research School of Astronomy and Astrophysics, The Australian National University, Mount Stromlo and Siding Spring Observatories, via Cotter Rd, Weston Creek PO 2611, Australia; brian@mso.anu.edu.au

⁵Cerro Tololo Inter-American Observatory, Casilla 603, La Serena, Chile; nsuntzeff@noao.edu, kkrisciunas@noao.edu, pcandia@ctiosz.ctio.noao.edu

⁶Harvard-Smithsonian Center for Astrophysics, 60 Garden Street, Cambridge, MA 02138; kirshner@cfa.harvard.edu, pchallis@cfa.harvard.edu, tmathe-son@cfa.harvard.edu

⁷Pontificia Universidad Católica de Chile, Departamento de Astronomía y Astrofísica, Casilla 306, Santiago 22, Chile; aclocchi@astro.puc.cl

⁸University of California, Berkeley, Department of Astronomy, 601 Campbell Hall, Berkeley, CA 94720-3411; alex@astro.berkeley.edu, weidong@astro.berkeley.edu, acoil@astro.berkeley.edu, sjha@astro.berkeley.edu

⁹University of Notre Dame, Department of Physics, 225 Nieuwland Science Hall, Notre Dame, IN 46556-5670; pgar-navi@miranda.phys.nd.edu, sholland@nd.edu

¹⁰University of Washington, Department of Astronomy, Box 351580, Seattle, WA 98195-1580; hogan@astro.washington.edu, stubbs@astro.washington.edu

¹¹Las Campanas Observatory, Casilla 601, La Serena, Chile; mmp@lco.cl

¹²European Southern Observatory, Karl-Schwarzschild-Strasse 2, Garching, D-85748, Germany; bleibund@eso.org, jspyromi@eso.org

¹³Space Telescope Science Institute, 3700 San Martin Drive, Baltimore, MD 21218; ariess@stsci.edu

¹⁴Stockholm Observatory, SCFAB, SE-106 91 Stockholm, Sweden; jesper@astro.su.se

¹⁵Deceased 12 December 2001

at $z \approx 0.5$ should produce a significant measurement of cosmic deceleration. Early results by Perlmutter et al. (1997) favored a large deceleration which they attributed to Ω_M near 1. But subsequent analysis of an augmented sample (Perlmutter et al. 1998) and independent work by the HZT (Garnavich et al. 1998a) showed that the deceleration was small, and far from consistent with $\Omega_M = 1$.

Both groups expanded their samples and both reached the surprising conclusion that cosmic expansion is accelerating (Riess et al. 1998a; Perlmutter et al. 1999). Cosmic acceleration requires the presence of a large, hitherto undetected component of the Universe with negative pressure: the signature of a cosmological constant or other form of “dark energy.” If this inference is correct, it points to a major gap in current understanding of the fundamental physics of gravity (e.g., Carroll 2001, Padmanabhan 2002). The consequences of these astronomical observations for theoretical physics are important and have led to a large body of work related to the cosmological constant and its variants. For astronomers, this wide interest creates the obligation to test and repeat each step of this investigation that concludes that an unexplained energy is the principal component of the Universe.

Formally, the statistical confidence in cosmic acceleration is high — the inference of dark energy is not likely to result simply from random statistical fluctuations. But systematic effects that change with cosmic epoch could masquerade as acceleration (Drell, Loredo, & Wasserman 2000; Rowan-Robinson 2002). In this paper we not only provide a statistically independent sample of well-measured supernovae, but through the design of the search and execution of the follow-up, we expand the redshift range of supernova measurements to the region $z \approx 1$. This increase in redshift range is important because plausible systematic effects that depend on cosmic epoch, such as the age of the stellar population, the ambient chemical abundances, and the path length through a hypothesized intergalactic absorption (Rana 1979, 1980; Aguirre 1999a,b) would all increase with redshift. But, for plausible values of Ω_Λ and Ω_M , 0.7 and 0.3 for example, the matter-dominated deceleration era would lie just beyond $z = 1$. As a result, the *sign* of the observed effect on luminos-

ity distance would change: at $z \approx 0.5$ supernovae are *dimmer* relative to an empty universe because of recent cosmic acceleration, but at $z \approx 1$ the integrated cosmological effect diminishes, while systematic effects are expected to be larger (Schmidt et al. 1998).

Confidence that the Universe is dominated by dark energy has been boosted by recent observations of the power spectrum of fluctuations in the cosmic microwave background (de Bernardis et al. 2002; Spergel et al. 2003). Since the CMB observations strongly favor $\Omega_{total} = 1$ to high precision (± 0.02), and direct measurements of Ω_M from galaxy clusters seem to lie around 0.3 (Peacock et al. 2001), mere subtraction shows there is a need for significant dark energy that is not clustered with galaxies. However, this argument should not be used as an excuse to avoid scrutiny of each step in the supernova analysis. Supernovae provide the *only* qualitative signature of the acceleration itself, through the relation of luminosity distance with redshift, and most of that effect is produced in the recent past, from $z = 1$ to the present, and not at redshift 1100 where the imprint on the CMB is formed. This is why more supernova data, better supernova data, and supernova data over a wider redshift range are needed to confirm cosmic acceleration. This paper is a step in that direction.

The most likely contaminants of the cosmological signal from SN Ia are luminosity evolution, gray intergalactic dust, gravitational lensing, or selection biases (see Riess 2000, Filippenko & Riess 2001, and Leibundgut 2001 for reviews). These have the potential to cause an apparent dimming of high-redshift SN Ia that could mimic the effects of dark energy. But each of these effects would also leave clues that we can detect. By searching for and limiting the additional observable effects we can find out whether these potential problems are important.

If luminosity evolution somehow made high-redshift SN Ia intrinsically dimmer than their local counterparts, supernova spectra, colors, rise times and light-curve shapes should show some concomitant effects that result from the different velocities, temperatures, and abundances of the ejecta. Comparison of spectra between low-redshift and high-redshift SN Ia (Coil et al. 2000) yields no significant difference, but the precision is low and

the predictions from theory (Höflich, Wheeler, & Thielemann 1998) are not easily translated into a limit on possible variations in luminosity. Some troubling differences in the intrinsic colors of the high and low-redshift samples have been pointed out by Falco et al. (1999) and Leibundgut (2001). Larger, well-observed samples, including the one reported here, will show whether this effect is real.

Gray dust that absorbs without producing as much reddening as Galactic dust could dim high-redshift SN Ia without leaving a measurable imprint on the observed colors. Riess et al. (1998a) argued that dust of this sort would need to dim distant supernovae by 0.25 mag at $z \approx 0.5$ in a matter-only universe. To produce the dimming we attribute to acceleration, dust would also increase the variance of the apparent SN Ia luminosities more than is observed. However, such dust, if smoothly dispersed between the galaxies, could appear degenerate with cosmic acceleration (Rana 1979, 1980; Aguirre 1999a,b). Aguirre's electromagnetic calculations of the scattering properties for intergalactic dust show that it can produce less reddening than galactic dust, but it cannot be perfectly gray. Near-infrared observations of one SN Ia at ≈ 0.5 (Riess et al. 2000) do not show the presence of this form of dust. Further observations over a wide wavelength range have been obtained by our team to construct a more stringent limit; these will be reported in a future paper (Jha et al. 2003a). Recent work by Paerels et al. (2002), which failed to detect X-ray scattering off gray dust around a $z = 4.3$ quasar, seems to indicate that gray, smoothly distributed, intergalactic dust has a density which is too low by a factor of 10 to account for the 0.25 mag dimming seen in the SN Ia Hubble diagram.

Selection biases could alter the cosmological inferences derived from SN Ia if the properties of distant supernovae are systematically different from those of the supernovae selected nearby. Simple luminosity bias is minor because the scatter in supernova luminosities, after correction for the light-curve shape, is so small (Schmidt et al. 1998; Perlmutter et al. 1999; Riess et al. 1998a). However, the nearby sample of SN Ia currently spans a larger range of extinctions and intrinsic luminosities than has been probed for SN Ia at $z \approx 0.5$. Most searches to date have only selected the tip of the iceberg: most supernovae at high redshift

lie below the sensitivity limit. We assume that we are drawing from the same population as nearby, but it would be prudent to test this rigorously. To make the SN evidence for dark energy robust against sample selection effects, we need more sensitive searches for SN Ia at $z \approx 0.5$ that could detect intrinsically dim or extinguished SN Ia so we can verify that the distant supernovae have a similar range of extinctions and intrinsic luminosities as the nearby sample. This was one goal of the 1999 search reported here.

Extending the data set to higher redshift is a more ambitious and difficult way to test for the cosmological origin of the observed dimming effect. Evolution or dust would most naturally lead to increased dimming at higher redshift, while cosmic deceleration in the early matter-dominated era ($z \geq 1.2$) would imprint the opposite sign on luminosity distances. A search at higher redshift demand that we search to fainter flux limits in bands that are shifted to the red to detect rest-frame B and V . In this paper, we describe a sensitive search in the R and I bands carried out at the Canada-France-Hawaii Telescope (CFHT) and at the Cerro Tololo Inter-American Observatory (CTIO) in 1999. For the highest redshifts, we detect flux emitted in the ultraviolet at the source. Members of the HZT have also embarked on an extensive study of the U -band properties of nearby supernovae that will help with the interpretation of these high-redshift objects (Jha 2003c).

Performing these tests requires searching for SN Ia with a deeper magnitude limit in redder bands than previous searches. This approach can sample the full range of extinctions and luminosities at $z \approx 0.5$ and test for a turn-down in the Hubble diagram at $z \geq 1$. Thus far, direct measurement of deceleration at early epochs rests in observations of one SN Ia, SN 1997ff, at the remarkably high redshift of ~ 1.7 . These observations match best with a dark-energy source for the observed behavior of SN Ia (Riess et al. 2001). But this single object represents just one data point isolated from the body of SN Ia observations — and there is evidence that this object could be significantly magnified by gravitational lensing (Benítez et al. 2002). A continuous sample from $z \approx 0.5$ through $z \approx 1$ out to $z \geq 1.5$ is required to make this crucial test convincing. The present paper represents a step in that direction by extending the sample

to $z \approx 1$. Future discoveries of very high- z supernovae using the Advanced Camera for Surveys on the *Hubble Space Telescope (HST)*, successfully installed in 2002, will help bridge the gap from the high-redshift end.

Section 2 of this paper describes the search, shows spectra of the supernovae, and provides our photometric results. Section 3 gives an account of the analysis including K-corrections, fits to the light curves, and luminosity distances. In §4 we discuss the inferred cosmological parameters, and in §5 we discuss how these results can be used to test for systematic errors in assessing cosmic acceleration from SN Ia observations. Some novel features of the analysis are described more thoroughly in the Appendix.

2. Observations

2.1. Search

The SN Ia reported here were discovered at the CFHT using the CFH-12K camera and at the CTIO 4-m Blanco telescope using the CTIO Mosaic camera. The CFH-12K camera provides $0''.206$ pixels and a field of view of 0.33 deg^2 , and the CTIO mosaic has $0''.270$ pixels with a field of view of 0.38 deg^2 .

We obtained templates in 1999 October and obtained subsequent images in November to find new objects, plausibly supernovae, with a rise time in the observer frame of ~ 1 month. On the nights of 1999 October 3 and 1999 October 7 (UT dates are used throughout this paper), we obtained CFH-12K images of 15 fields (5 deg^2) in the I and R bands with median seeing of $0''.65$ and $0''.72$, respectively. We integrated for a total of 60 minutes on 6 of the I -band fields and 3 of the R -band fields, and 30 minutes on the rest. Each integration was of 10 minutes duration, with the frames dithered by small offsets to help in removing cosmic rays and CCD defects. The photometric zero-points were approximately $I = 35.0$ and $R = 35.6$ mag for the 60 minute exposures — in other words, a source of that magnitude would produce 1 e^- . This permits detection of stars with $m = 24$ mag at a signal-to-noise ratio (S/N) of 12 and 16, respectively, or detection of a supernova with $m = 24$ mag at a S/N of 9 and 11 in a difference search. A first-epoch search scheduled in October at CTIO was clouded out.

Despite a generous time allocation, we ran into difficulties at CFHT a month later because of weather. The first night (1999 November 2) had clouds and bad seeing ($> 1''$). We accumulated 60 minutes in the I band for each of 8 fields, but only one of these fields contributed to the search, yielding one SN Ia: SN 1999ff. The second night (1999 November 3) had a mean extinction of about 0.5 mag from clouds, but the seeing was very good (median $0''.59$). We obtained reasonably good data in the I band for 8 fields, with integrations of 60 minutes for five of these, and 30 minutes for three. Three nights later (1999 November 6) we searched at CTIO, using R -band observations from CFHT as the first-epoch observations. Although the CTIO data enabled us to confirm the SN Ia found in the I band at CFHT, and produced several candidates that required spectroscopic follow-up, we found no new supernovae from these observations. Spectra of several CTIO candidates revealed the disappointing fact that our attempt to compare November CTIO observations with October CFHT templates produced subtly false candidates where a mismatch between the CFHT and CTIO filters caused the difference between the two to give the illusion of a new objects appearing between October and November. In fact, these were M stars or emission-line galaxies whose $H\alpha$ emission line fell at the red end of the R -band filter. Only the comparison of CFHT data with CFHT templates provided genuine detections of supernovae.

Our reduction and search procedure, detailed by Schmidt et al. (1998), consists of bias subtraction, flatfielding, subtraction of I -band fringes, masking bad columns, and finally combining dithered images to reject cosmic rays and moving objects. In each field, we identified stars, performed an astrometric solution, and then remapped the image onto a common coordinate system. (This mapping is flux conserving but uses a Jacobian to restore the photometric accuracy that is destroyed by flatfielding.) For each pair of images of a field, from the first (October) and second (November) epoch, we then used the algorithms described by Alard & Lupton (1998) to convolve the image with the better seeing into agreement with the worse image. Next we matched the flux levels and subtracted.

These difference images were then searched au-

tomatically for residuals resembling the point-spread function (PSF), with possible SN Ia flagged for further inspection by humans. Simultaneously, we searched all image pairs by inspecting the difference images by eye. We found little difference in the detection efficiency between the semi-automatic approach and inspection by experienced observers. For all the SN Ia candidates, we inspected each of the individual exposures to ensure that the putative SN Ia was not a cosmic ray, moving object, or CCD flaw. All 37 final candidates were tabulated along with estimated I and R magnitudes (from the CTIO observations), including the properties of the possible host galaxy and distance from the center of the host. This candidate list became our observing list for subsequent spectroscopic investigation.

Different exposure times in different fields, variable extinction due to clouds, changes in seeing, and sensitivity variations among the chips in the CFH-12K mosaic make it hard to quantify a single detection threshold for genuine events in this search. We believe that, overall, our search is 95% effective for objects brighter than $I = 23.5$ mag, and substantially better than 50% at $I = 24$ mag. In some favorable cases we found objects as faint as $I = 24.5$ mag.

We began observing our 37 candidate objects at the Keck-II telescope on 1999 November 8. Our aim was to determine the nature of each object and to measure its redshift. Of these 37, two turned out to be active galactic nuclei at redshifts of 1.47 and 1.67; one was an M star and two were galaxies with $H\alpha$ emission admitted because of mismatched R filters; five had disappeared, suggesting either that the discovery was well past maximum or the detection was spurious; four were judged to be Type II supernovae from spectra or blue color; two were too bright to be of interest for our purposes, $I \approx 21$ mag in bright host galaxies, possibly nearby SN II, for which we did not spend time to get spectra; three were SN Ia with $0.3 < z < 0.7$ which we chose not to follow; seven were faint candidates for which we did not have time to get spectra; and 11 were the candidate SN Ia which we chose to follow. These are shown in Figure 1. The selection of objects was based on color information (we chose objects with colors consistent with SN Ia with any amount of reddening, in the range $0.1 < z < 1.5$); the amount of variation of the

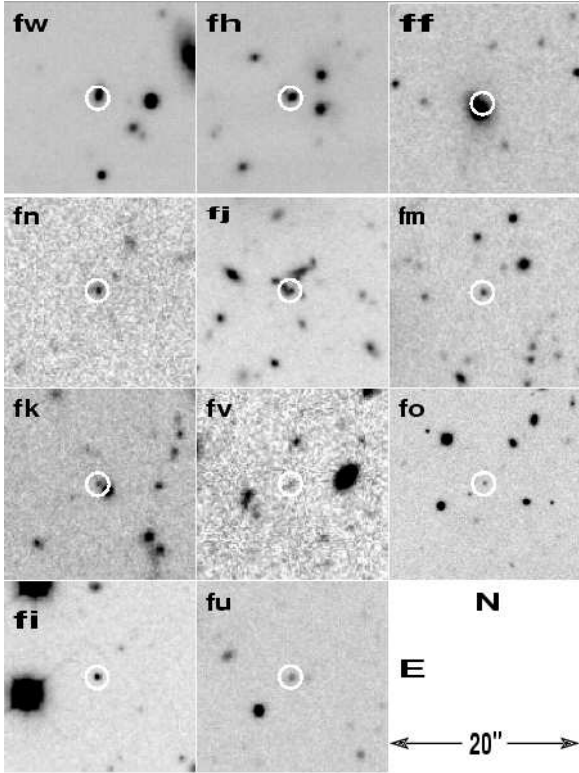


Fig. 1.— Host galaxies for the eleven supernovae. Each image is $20''$ on a side and taken from an average of several I-band frames. A $2''$ radius circle marks the position of the supernova. North is at the top and east to the left in each image.

SN, with preference to objects that were not seen in the previous epoch, but that had varied significantly; the host-galaxy brightness at the supernova position, avoiding supernova candidates on extremely bright backgrounds; and host brightness/size — avoiding supernovae in low redshift galaxies ($z < 0.1$). These selection effects are all undesirable, but with limited telescope time, they were necessary compromises to achieve the goals of the search.

Table 1 lists the J2000 coordinates of the SN Ia, the Galactic extinction from Schlegel, Finkbeiner, & Davis (1998), the number of photometric observations in various bandpasses accumulated from various telescopes, the modified Julian date of maximum light, and our nickname for the supernova, assigned before there was a designation for each event in the IAU Circulars (see Tonry et al.

1999). The last three objects on the list are real objects which we pursued, but based on our spectra and subsequent light curves, the evidence is too weak to consider them SN Ia. SN 1999fi (Boris) was very close to SN 1999fj, so it did not cost extra observing time to get photometry, but the other two (SN 1999fo and SN 1999fu) fooled us into making 22 photometric observations and expending many hours of Keck time to get spectra that were, in the end, inconclusive. Although these two are real events, with a definite flux increase from October to November and a decrease in flux after November, we have not shown they are SN Ia, and they are not included in the analysis.

2.2. Spectral Observations and Reductions

We obtained spectra of our SN Ia candidates with LRIS (Oke et al. 1995) on the Keck-II telescope during five nights between 1999 November 8 and 14. The seeing varied from $0''.8$ to $1''.1$ during the first three nights and was $\sim 0''.5$ on the last two nights. We used a $1''.0$ slit for all of our observations, except for SN 1999fv where we used a $0''.7$ slit on one night. We used a 150 line mm^{-1} grating for the first half of the run, then switched to a 400 line mm^{-1} grating for the second half in order to better remove night-sky lines. The resulting spectral resolution is $\sim 20 \text{ \AA}$ for the 150 line mm^{-1} grating and $\sim 8 \text{ \AA}$ for the 400 line mm^{-1} grating. The pixel size for the 150 and 400 line mm^{-1} gratings is $\sim 5 \text{ \AA pix}^{-1}$ and $\sim 2 \text{ \AA pix}^{-1}$, respectively. The total exposure times for each SN Ia are listed in Table 2. We moved the object along the slit between integrations to reduce the effects of fringing. The slit was oriented either near the parallactic angle, or to include the nucleus of the host galaxy or a nearby bright star to provide quantifiable astrometry along the slit and to define the trace of a source along the spectral direction.

When using the 150 line mm^{-1} grating, internal flatfield exposures and standard stars were observed both with and without an order-blocking filter to remove contamination from second-order light. For the high- z SN Ia observations no order-blocking filter was needed, as there is very little light from the object or from the sky below an observed wavelength of 4000 \AA . We used BD+17 $^{\circ}$ 4708 as a standard star for the first two nights and Feige 34 (Massey et al. 1988) for

TABLE 1
FALL 1999 OBSERVATIONS

SN name	RA (J2000)	Dec (J2000)	$E(B-V)$	N_{obs}	MJD_{max}	Nickname
SN 1999fw	23:31:53.03	+00:09:32.3	0.039	25	51482	Nell
SN 1999fh	02:27:58.33	+00:39:36.8	0.031	15	51488	Fearless Leader
SN 1999ff	02:33:54.39	+00:32:55.6	0.026	25	51494	Bashful
SN 1999fn	04:14:03.88	+04:17:55.0	0.326	46	51498	Scooby Doo
SN 1999fj	02:28:23.72	+00:39:09.6	0.030	20	51475	Natasha
SN 1999fm	02:30:35.62	+01:09:43.3	0.023	21	51488	Fred
SN 1999fk	02:28:53.88	+01:16:24.2	0.030	22	51492	Velma
SN 1999fv	23:30:35.80	+00:16:40.0	0.041	8	51457	Dudley Doright
SN 1999fo	04:14:45.75	+06:38:34.3	0.291	11	...	Gertie
SN 1999fi	02:28:11.67	+00:43:39.3	0.031	12	...	Boris
SN 1999fu	23:29:48.21	+00:08:27.0	0.048	11	...	Alvin

the last three nights. Standard CCD processing and optimal spectral extraction were done with IRAF¹⁶. We used our own IDL routines to calibrate the wavelengths and fluxes of the spectra and to correct for telluric absorption bands. For SN Ia that were observed on more than one night, the data were binned to the larger pixel size if different gratings were used, scaled to a common flux level, and combined with weights depending on the exposure time to form a single spectrum.

2.3. SN Ia Spectra and Redshifts

The SN Ia spectra are shown in Figure 2 at their observed wavelengths. For each SN Ia we list in Table 2 the redshift, the supernova type, the number of nights observed with Keck, the total exposure time, and an explanation of how the redshift was derived. For SN Ia with narrow emission or absorption lines from the host-galaxy light, we determined the redshift by using the centroid of the line(s) with a Gaussian fit. For the three SN Ia spectra without narrow lines from the host galaxy, we use the broad SN Ia features to determine the redshift by cross-correlating the high- z spectrum with low- z SN Ia spectra obtained near maximum light. We also include galaxy and M-star spec-

tra among our templates for cross-correlation with spectra without narrow emission lines. Errors on the redshifts are ± 0.001 (1σ) when based on a narrow line and ± 0.01 when based on broad SN Ia features. The redshift of SN 1999fv has a large uncertainty (1.17–1.22) due to the low S/N of the spectrum (see Coil et al. 2000 for further discussion).

Figure 3 presents the high- z spectra smoothed with a Savitsky-Golay filter of width 100 Å, sorted by redshift, with the lowest- z SN Ia at the top. This polynomial smoothing filter preserves line features better than boxcar smoothing, which damps out peaks and valleys in a spectrum. The width of the smoothing filter is apparent in the [O II] $\lambda 3727$ emission line seen in many of the spectra. We also plot two low- z SN Ia (SN 1989B, Wells et al. 1994; SN 1992A, Kirshner et al. 1993) and a low- z SNIc [SN 1994I dereddened by $E(B-V) = 0.45$ mag; Filippenko et al. 1995] for comparison, all with ages before or at maximum light. Features which distinguish a SN Ia (Filippenko 1997) are deep Ca II H&K absorption near 3750 Å, the Si II $\lambda 4130$ dip blueshifted to 4000 Å, and Fe II $\lambda 4555$ and/or Mg II $\lambda 4481$, the combination of which create a distinct double-bump feature centered at 4000 Å. For the lower- z spectra we have enough wavelength coverage to see 6150 Å, where the Si II $\lambda 6355$ absorption feature is prominent in SN Ia, but beyond $z \approx 0.4$ this

¹⁶IRAF is distributed by the National Optical Astronomy Observatories, which are operated by the Association of Universities for Research in Astronomy, Inc., under cooperative agreement with the National Science Foundation

feature becomes difficult to detect. Early SNIc spectra look similar to SN Ia blueward of 5000 Å, but lack the prominent Si II dip at 4000 Å which leads to the double-bump feature seen only in SN Ia.

SN 1999fw, 1999fh, 1999ff, 1999fn, and 1999fj are all clearly SN Ia. SN 1999fm is a Type I SN, but we cannot distinguish from the spectrum alone whether it is a Type Ia or Ic. SN 1999fk shows a definite rise around 4000 Å and has some hints of a double peak at this location, but is not definitively a SN Ia. SN 1999fv shows some bumps centered at 4000 Å, which, as discussed in Coil et al. (2000), are plausibly SN Ia features at a redshift of ~ 1.2 . All eight of these supernovae are used in this paper.

SN 1999fi, 1999fu, and 1999fo do not show any SN features in their spectra. For each of these systems, we have a redshift; for SN 1999fi and 1999fu this comes from a single line we assume to be [O II] $\lambda 3727$. For SN 1999fo the spectrum appears to have Ca II H&K absorption at $z = 1.07$. As stated above, these three objects are not used in the analysis.

2.4. Properties of the Host Galaxies

Host galaxies and the environment around each supernova are shown in Figure 1. The images are the average of the *I*-band images with the best seeing. No host was detected for SN 1999fm. SN 1999fj appears in a small group of galaxies and its host is assumed to be the elongated galaxy just east of the supernova. Host magnitudes were measured from images taken after the supernova had faded. For the brightest hosts, the flux was summed out to an isophote of 26 mag/square-arcsec, but for the faint hosts the flux was summed in a 4'' diameter aperture. The results, without correction for extinction, are given in Table 3.

Offsets between the supernovae and their hosts are also given in Table 3, as is the projected separation in kpc assuming a flat Λ -dominated cosmology with $\Omega_M = 0.3$. The distribution of projected separations for these new supernovae is narrower than that of earlier searches (Farrah et al. 2002), meaning our supernovae were discovered closer to the hosts. This may be due to the greater depth of this search and better image quality as it attempted to detect objects at $z > 1$.

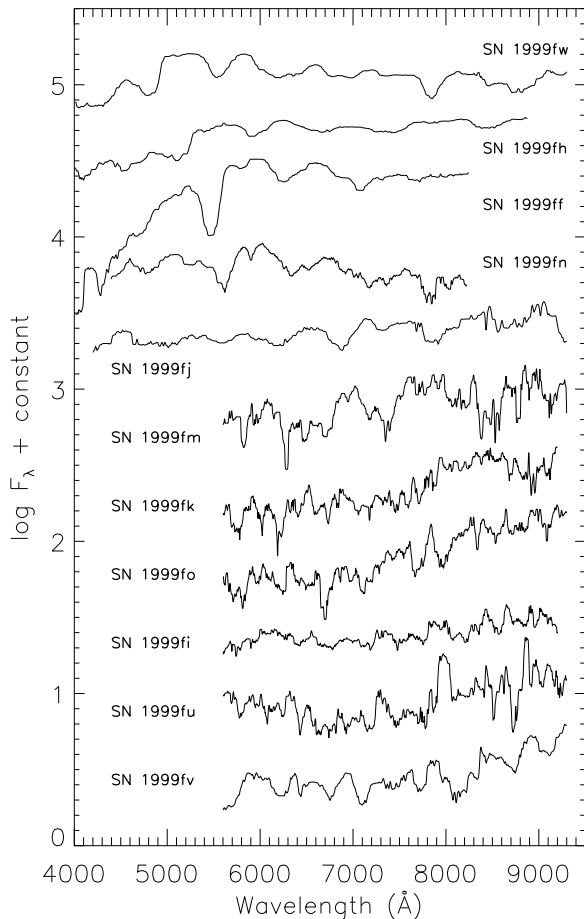


Fig. 2.— High- z supernova spectra shown at their observed wavelengths, smoothed by a 32-pixel running median and a Gaussian of 4-pixel sigma.

2.5. Photometric Calibrations and Reductions

The photometric data gathered of the supernovae discovered at CFHT and CTIO came from a wide variety of instruments and telescopes including Keck LRIS, Keck ESI, Keck NIRC, VLT FORS, VLT ISAAC, UKIRT UFTI, UH 2.2-m, VATT, WIYN, and *HST*. We accumulated a total of 216 observations of our 11 candidate SN Ia over the span of approximately one year, in the *V*, *R*, *I*, *Z*, and *J* bandpasses, totaling ~ 200 hours of exposure time. The seeing of the combined, remapped images had a median of 0''.83, with quartiles at 0''.72 and 1''.04.

Calibration of these data turned out to be espe-

TABLE 2
FALL 1999 SPECTROSCOPIC DATA

SN name	z	Type	# nights	Exp. (sec)	z determination
SN 1999fw	0.278	Ia	1	1200	broad SN features
SN 1999fh	0.369	Ia	1	1800	[O II] λ 3727 in SN spectrum
SN 1999ff	0.455	Ia	1	2200	Balmer lines in galaxy spectrum
SN 1999fn	0.477	Ia	2	5900	[O II] λ 3727 in SN spectrum
SN 1999fj	0.816	Ia	1	3600	[O II] λ 3727 in SN spectrum
SN 1999fm	0.95	Ia?	2	6600	broad SN features
SN 1999fk	1.057	Ia?	2	7000	[O II] λ 3727 in SN spectrum
SN 1999fv	1.17-1.22	Ia	2	10000	broad SN features
SN 1999fo	1.07	?	3	14200	Ca H&K dip in spectrum
SN 1999fi	1.10	?	1	5000	[O II] λ 3727 in spectrum
SN 1999fu	1.135	?	2	7200	[O II] λ 3727 in spectrum

TABLE 3
FALL 1999 HOST GALAXIES^a

SN name	Host R	Host I	Host Z	Offset (")	Proj. Sep. (kpc)
SN 1999fw	21.1	20.4	...	0.51	2.3
SN 1999fh	21.2	20.8	20.5	0.03	0.2
SN 1999ff	19.9	19.2	19.1	2.01	12.6
SN 1999fn	24.5	23.5	...	0.31	2.0
SN 1999fj	23.3	22.3	21.9	0.89	7.2
SN 1999fm	...	> 24.5
SN 1999fk	...	21.9	23.7	1.36	11.9
SN 1999fv	> 26.0	25.8	...	0.30	2.7
SN 1999fo	...	23.1	23.2	0.19	1.7
SN 1999fi	24.8	23.1	22.9	0.16	1.4
SN 1999fu	24.2	23.6	23.5	0.35	3.1

^aThe offset is the angular separation between the SN and host in arcsec, and the projected separation is in kpc. SN 1999fm had no detectable host. Ellipsis indicate no image available in that band.

cially challenging, due to a variety of difficulties. The photometric calibration of stellar sequences near our SN Ia was intended to come from observations with the UH 2.2-m and the CTIO 1.5-m telescopes. To this end, we observed Landolt (1992) standards in V , R , I , and Z on a variety of photometric nights, and also observed our SN Ia fields to establish the magnitudes of local photometric reference stars. We took a sequence of short exposures of a constant flatfield to establish the shutter timing error, and checked the linearity of the CCD by exposures of different duration. For standard-star reductions we summed the flux (with background subtraction) of each star through a $14''$ aperture, and calculated an atmospheric extinction term for each night. A typical scatter in this fit to airmass and color was 0.02 mag, and arises from the usual causes: sky errors, imperfect flatfielding, changes in atmospheric transparency, CCD non-linearity, shutter timing errors, and PSF or scattered-light variations. In the case of the UH 2.2-m data, there were some observations which deviated significantly from the root-mean-square (*rms*) error of the majority of data. This was eventually tracked down to an error in dome control, causing observations to be vignetted by the dome shutter. The UH 2.2-m data are therefore not completely reliable photometric calibrations. The CTIO 1.5-m data had no such problems, and were taken on absolutely photometric nights. However, they do not cover all fields, and the overlap in brightness between data with high photometric accuracy from the 1.5-m and the unsaturated data from the larger telescopes was not large.

To bridge these calibration difficulties, we combined two additional calibration sources, the Sloan Digital Sky Survey (SDSS) (Stoughton et al. 2002) and the 2001 HZT campaign (Barris et al. 2002). The 2001 HZT campaign took great pains to obtain very high accuracy photometry at the CTIO 1.5-m telescope, which was reduced in a manner identical to the 1999 CTIO data, as described above. These observations of more than 200 stars were used to calibrate a catalog of R , I , and Z photometry of about 4000 stars near $\alpha = 02^h 28^m$, $\delta = +00^\circ 35'$, derived from CFHT+12K mosaic images. The R and I bandpasses of these data were transformed to the standard Kron-Cousins system (Kron & Smith 1951; Cousins 1976), us-

ing the CTIO derived values, and the Z band was transformed to the CTIO system, as described below.

This 2001 HZT catalog and all of our supernovae at $RA = 23^h$ and 02^h are encompassed by the SDSS catalog. Using the matched stars at 02^h between our 2001 HZT photometric catalog and the SDSS (using PSF-derived magnitudes of the Sloan data — not the default available on the website), we derived the following transformations from the SDSS g' , r' , i' , and z' magnitudes and our Vega-based magnitudes:

$$V - g' = +0.172 - 0.745(g' - r'),$$

$$R - r' = -0.122 - 0.316(r' - i'),$$

$$I - i' = -0.423 - 0.378(i' - z'),$$

$$Z - z' = -0.511 - 0.037(r' - i'),$$

$$Z - z' = -0.508 - 0.267(r' - i') + 0.424(i' - z').$$

The two-color fit to $Z - z'$ is slightly better, but obscures the fact that Z and z' are nearly identical, apart from a zero-point offset.

For all colors, the scatter in the transformation for individual stars (which are not dominated by shot noise like the faint SDSS stars, or by saturation like the CFHT stars of roughly the same magnitude) is approximately 0.02 mag *rms*. These transformations enable us to calibrate the R , I , and Z 1999 CFHT survey fields via the SDSS early-release data.

Since we did not observe in the V band during our Fall 2001 campaign, we needed extra steps to derive the calibration of the V observations for our 1999 data. We used Landolt (1992) stars in our fields and derived a satisfactory relation for $0 < (R-I) < 1$ mag:

$$(V-R) = -0.024 + 1.104(R-I).$$

For redder stars, there are significant differences in the V -band colors for giants and dwarfs, which we sought to avoid. This relation allowed us to produce “ V ” magnitudes for the Fall 2001 catalog, using the R and I magnitudes. We then compared the stars that were also available from SDSS, and derived a g' to V transformation. While individual stars can have substantial errors via these transformations, in the mean of hundreds of stars that

we used these transformations are better than 0.01 mag.

The Z band was both important and problematic for us. At $z > 1$, the rest-frame B band starts to shift beyond the observer's I band, and the systematics of rest-frame U -band observations were not yet well established at the time of these observations (but see Jha 2003c), so we needed a color for our SN Ia based on bandpasses redder than I . There is a variety of Z bands; ours is a Vega-normalized bandpass defined by the CTIO natural system (RG850, two aluminum reflections, atmosphere, and a SITe CCD red cutoff), and it is quite well described as a sum of two Gaussians, one centered at 8800 Å with a full-width at half-maximum (FWHM) of 280 Å and a height of 0.86, and the other at 9520 Å with a FWHM of 480 Å and a height of 0.41. The Z bandpass and this approximation are illustrated in Figure 4. Our Z -band observations were calibrated by observing a series of Landolt stars, whose magnitudes were derived by integrating their spectrophotometry (N. Suntzeff, in preparation) with this bandpass. This system is defined to have $(V - Z) = 0$ mag for Vega.

The SDSS observations covered all our fields except for those containing SN 1999fn and SN 1999fo. For all SN Ia, except these two, we extracted SDSS stars which fell within the supernova fields, and used the above relations to produce Johnson/Kron-Cousins magnitudes for each star. For SN 1999fn and SN 1999fo, we used our UH 2.2-m photometric observations, verified with a few overlapping stars from the 1999 CTIO 1.5-m observations, to set the R and I magnitudes of a stellar sequence around the SN. The V, Z magnitudes were set using color relations derived above. As stated above, these transformations, while good in the mean, may not be appropriate for unusual stars (or quasars), and consequently, our derived magnitudes are based relative to the sequence of stars, rather than weighting any individual star too highly. The adopted standard-star sequences in the vicinity of each supernova are given in Table 4. This calibration procedure is far from ideal, but cross-checks suggest it is as good as the Sloan zero-point uncertainty, 0.04 mag.

We calibrated the J -band data from VLT and UKIRT using observations of ten standard stars from Persson et al. (1998). The Keck data were

calibrated by transferring the photometric zero-points from the UKIRT observations to a galaxy in the field of SN 1999fn.

TABLE 4
LOCAL STANDARD STARS

SN name	RA	Dec	V	\pm	R	\pm	I	\pm	Z	\pm
SN1999fu	23:29:46.8	+00:11:11	21.43	0.04	20.25	0.06	18.57	0.03	17.92	0.04
	23:29:46.5	+00:04:45	20.70	0.03	19.69	0.04	18.42	0.03	17.93	0.04
	23:29:45.4	+00:09:08	20.74	0.03	19.77	0.04	18.52	0.03	18.05	0.05
	23:29:41.7	+00:10:18	19.40	0.02	18.87	0.03	18.36	0.03	18.20	0.05
	23:29:41.3	+00:11:08	18.58	0.02	18.46	0.02	18.37	0.03	18.37	0.06
	23:29:37.8	+00:05:06	20.73	0.03	19.80	0.04	18.79	0.04	18.40	0.06
	23:29:37.5	+00:10:26	20.99	0.04	19.94	0.05	18.42	0.03	17.82	0.04
	23:29:35.3	+00:10:06	20.94	0.03	19.87	0.05	18.45	0.03	17.89	0.04
SN1999ff	02:34:00.2	+00:34:20	20.03	0.02	18.99	0.03	17.62	0.02	17.08	0.03
	02:33:54.2	+00:29:53	19.37	0.02	18.87	0.03	18.38	0.03	18.21	0.05
	02:33:51.7	+00:29:48	18.71	0.02	17.88	0.02	16.96	0.02	16.62	0.02
	02:33:57.1	+00:31:18	19.90	0.02	19.10	0.03	18.31	0.03	18.02	0.04
	02:33:53.3	+00:28:18	19.71	0.02	18.79	0.03	17.74	0.02	17.33	0.03
	02:33:46.5	+00:27:08	20.85	0.03	19.70	0.04	18.02	0.03	17.36	0.03
	02:33:36.6	+00:28:39	20.02	0.03	19.29	0.03	18.56	0.03	18.30	0.06
	02:33:55.0	+00:28:02	20.01	0.02	19.10	0.03	18.02	0.03	17.61	0.03
SN1999fi	02:28:24.4	+00:42:08	19.96	0.02	19.12	0.03	18.26	0.03	17.94	0.04
	02:28:17.3	+00:39:06	21.20	0.04	20.02	0.05	18.36	0.03	17.70	0.04
	02:28:20.5	+00:46:42	20.49	0.03	19.58	0.04	18.50	0.03	18.09	0.05
	02:28:10.9	+00:37:53	21.38	0.05	20.33	0.07	18.90	0.04	18.33	0.06
	02:28:13.2	+00:38:32	20.03	0.03	19.53	0.04	19.07	0.05	18.91	0.10
	02:28:01.1	+00:42:07	21.64	0.06	20.58	0.08	19.14	0.05	18.57	0.07
	02:28:10.6	+00:46:24	21.27	0.05	20.36	0.07	19.31	0.06	18.91	0.09
	02:28:20.3	+00:39:40	21.72	0.06	20.74	0.10	19.46	0.06	18.96	0.10
SN1999fv	23:30:39.0	+00:19:24	19.77	0.03	19.36	0.03	18.89	0.04	18.73	0.08
	23:30:20.7	+00:17:28	19.20	0.02	18.85	0.03	18.39	0.03	18.24	0.05
	23:30:45.7	+00:17:16	20.62	0.03	19.69	0.04	18.53	0.03	18.07	0.05
	23:30:29.0	+00:12:18	19.44	0.02	18.96	0.03	18.55	0.03	18.42	0.06
	23:30:33.9	+00:16:19	21.86	0.07	20.82	0.10	19.31	0.06	18.70	0.08
	23:30:39.8	+00:14:41	21.36	0.05	20.45	0.07	19.26	0.05	18.80	0.09
	23:30:24.3	+00:18:58	22.01	0.07	20.86	0.11	19.09	0.05	18.38	0.06
	23:30:46.6	+00:20:25	21.80	0.06	20.60	0.09	18.96	0.04	18.31	0.06
SN1999fh	02:28:04.7	+00:40:21	19.32	0.02	18.79	0.03	18.27	0.03	18.09	0.05
	02:28:01.6	+00:44:19	22.64	0.09	21.11	0.14	19.23	0.05	18.47	0.06
	02:28:01.1	+00:42:07	21.64	0.06	20.58	0.08	19.14	0.05	18.57	0.07
	02:27:58.6	+00:35:55	21.92	0.07	20.82	0.10	19.21	0.05	18.57	0.07
	02:28:02.6	+00:40:23	19.90	0.03	19.35	0.03	18.79	0.04	18.60	0.07
	02:28:05.7	+00:41:12	22.54	0.11	21.38	0.17	19.65	0.07	18.96	0.10
	02:28:06.7	+00:41:30	21.87	0.07	20.79	0.10	19.48	0.07	18.97	0.10
	02:27:58.6	+00:35:46	21.62	0.06	20.76	0.10	19.78	0.08	19.41	0.15
SN1999fm	02:30:31.2	+01:07:49	19.15	0.02	18.27	0.02	17.29	0.02	16.92	0.03
	02:30:39.4	+01:07:56	20.15	0.03	19.18	0.03	18.03	0.03	17.58	0.03

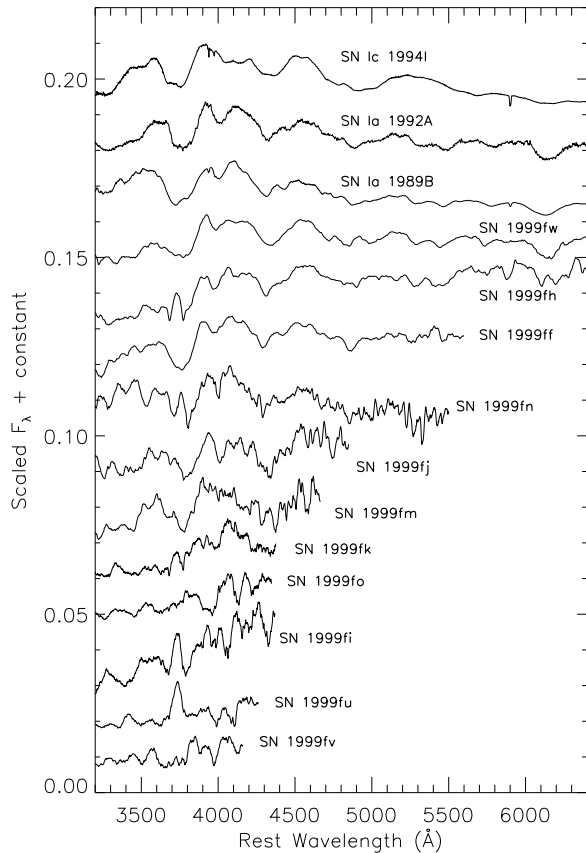


Fig. 3.— High- z SN spectra, shifted to rest wavelengths, smoothed by a Savitsky-Golay filter with a width of 100 \AA and compared to two low- z SN Ia (SN 1992A and SN 1989B) and a low- z SNIc (SN 1994I). The high- z SN spectra are shown sorted by redshift, with the lowest- z SN at the top. Based on these spectra, we cannot conclude that SN 1999fi, 1999fo, and 1999fu are SN Ia.

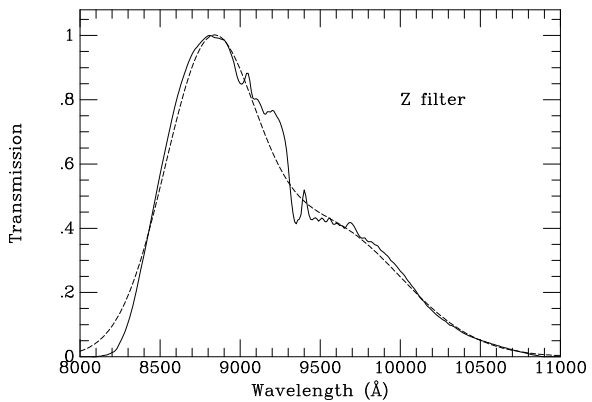


Fig. 4.— Z bandpass used for these observations. The dashed line is an approximation of the actual transmission, made up of two Gaussians as described in the text.

TABLE 4—*Continued*

SN name	RA	Dec	V	\pm	R	\pm	I	\pm	Z	\pm
	02:30:41.5	+01:08:03	21.02	0.03	19.90	0.05	18.44	0.03	17.86	0.04
	02:30:26.3	+01:08:59	17.56	0.02	17.05	0.02	16.57	0.02	16.41	0.02
	02:30:25.6	+01:09:21	19.62	0.02	18.48	0.02	16.80	0.02	16.14	0.02
	02:30:46.3	+01:09:31	20.66	0.03	19.58	0.04	18.16	0.03	17.61	0.03
	02:30:24.2	+01:10:57	20.93	0.03	19.89	0.05	18.47	0.03	17.91	0.04
	02:30:37.7	+01:12:00	19.01	0.02	18.03	0.02	16.88	0.02	16.44	0.02
SN1999fo	04:14:46.4	+06:38:46	18.87	0.03	17.40	0.03	17.28	0.03
	04:14:40.4	+06:39:46	19.17	0.03	17.74	0.03	17.61	0.03
	04:14:41.4	+06:38:40	21.09	0.03	18.26	0.03	17.91	0.03
	04:14:49.6	+06:37:35	19.45	0.02	18.30	0.03	18.25	0.03
	04:14:46.5	+06:38:29	20.13	0.02	18.81	0.03	18.74	0.03
	04:14:42.8	+06:37:52	22.04	0.07	19.14	0.03	18.77	0.03
	04:14:43.6	+06:37:23	21.61	0.05	19.08	0.03	18.81	0.03
	04:14:45.6	+06:37:47	21.60	0.05	19.12	0.03	18.86	0.03
SN1999fj	02:28:13.9	+00:39:05	19.80	0.02	18.77	0.03	17.46	0.02	16.94	0.03
	02:28:28.1	+00:38:25	20.81	0.03	19.71	0.04	18.05	0.03	17.40	0.03
	02:28:17.3	+00:39:06	21.20	0.04	20.02	0.05	18.36	0.03	17.70	0.04
	02:28:26.5	+00:40:53	20.86	0.03	19.78	0.04	18.33	0.03	17.76	0.04
	02:28:19.0	+00:36:59	21.83	0.06	20.69	0.09	19.05	0.05	18.41	0.06
	02:28:31.7	+00:37:01	20.79	0.03	19.89	0.05	18.89	0.04	18.51	0.07
	02:28:15.7	+00:40:27	23.91	0.30	22.51	0.48	19.86	0.09	18.78	0.08
	02:28:20.3	+00:39:40	21.72	0.06	20.74	0.10	19.46	0.06	18.96	0.10
SN1999fw	23:31:36.2	+00:15:10	21.19	0.04	20.00	0.05	18.24	0.03	17.54	0.03
	23:31:37.3	+00:10:14	18.92	0.02	18.50	0.02	18.09	0.03	17.95	0.04
	23:31:56.4	+00:15:47	21.19	0.04	20.24	0.06	19.18	0.05	18.77	0.08
	23:32:01.7	+00:13:41	21.61	0.05	20.55	0.08	18.95	0.04	18.31	0.06
	23:31:58.0	+00:14:12	20.69	0.03	19.67	0.04	18.27	0.03	17.72	0.04
	23:31:58.3	+00:13:09	20.57	0.03	19.51	0.04	18.21	0.03	17.71	0.04
	23:31:52.6	+00:09:32	20.22	0.03	19.56	0.04	18.89	0.04	18.66	0.08
	23:31:59.9	+00:11:08	20.79	0.03	19.66	0.04	18.07	0.03	17.45	0.03
SN1999fn	04:14:09.2	+04:19:06	18.35	0.03	17.79	0.03	17.19	0.03	17.19	0.03
	04:13:59.9	+04:18:46	19.47	0.03	18.24	0.03	16.74	0.03	16.44	0.03
	04:14:07.8	+04:19:15	19.40	0.03	18.24	0.03	17.14	0.03	16.91	0.03
	04:13:59.7	+04:19:08	19.90	0.05	18.68	0.03	17.42	0.03	17.11	0.03
	04:14:07.9	+04:17:58	19.92	0.02	18.75	0.03	17.60	0.03	17.37	0.03
	04:14:05.6	+04:17:40	20.67	0.03	19.41	0.03	18.08	0.03	17.79	0.03
	04:13:58.6	+04:16:37	20.81	0.04	19.63	0.03	18.20	0.03	17.88	0.03
	04:14:02.0	+04:17:41	21.22	0.05	19.94	0.03	18.51	0.03	18.20	0.03
SN1999fk	02:28:48.2	+01:16:17	19.33	0.02	18.43	0.02	17.43	0.02	17.05	0.03
	02:28:45.6	+01:15:39	19.96	0.02	18.90	0.03	17.47	0.02	16.91	0.03
	02:29:01.1	+01:13:42	21.89	0.06	20.57	0.08	18.59	0.03	17.80	0.04
	02:28:54.6	+01:14:43	20.79	0.03	19.86	0.05	18.81	0.04	18.41	0.06

All our supernova images were compared with the above stellar sequences to derive zero-points. The star fluxes were obtained using the Vista “psf” routine, which sums up the light within a radius of 20 pixels around a star, subtracts a fitted sky value, and rejects contamination from neighboring objects. Comparison of the fluxes and magnitudes, with due regard for saturation and magnitude errors, gave us a flux-magnitude zero-point and error for most images. For *HST* images, we used the precepts of Dolphin (2000) to convert fluxes to magnitudes.

2.6. Photometry of SN Ia

Our reductions of deep supernova observations obtained after the candidates were identified are very similar to the reductions carried out during the search. After bias subtraction, flatfielding, *I*-band and *Z*-band fringe correction, masking bad columns, and combination of dithered images while rejecting cosmic rays and moving objects, we identified stars relative to a fiducial image and performed an astrometric solution. We remapped a 1024×1024 pixel subarray of the source image onto a tangent plane coordinate system with $0''.2$ pixels. The *HST* observations had a small enough field of view and large enough distortion that some amount of star selection by hand was necessary to obtain a satisfactory astrometric match.

We had expected to use *HST* to acquire very high-quality light curves for a subset of our objects, but the gyro failure in Fall 1999 made *HST* unavailable until after this group of SN Ia had disappeared. We did succeed in using *HST* to get template observations of the host galaxies after the supernovae had faded for most of our targets. Late-time templates are very helpful to subtract the host galaxy accurately and to set the SN Ia flux zero-point.

Most modern supernova light curves are derived by subtraction of a template image taken before the supernova explosion or long after, so that it carries no supernova flux. While this sets a good flux zero-point for the subtraction, it also inflicts a common, systematic flux error on the light curve which can be substantial if the template observation has poor S/N or very different seeing.

To avoid these correlated errors, we subtracted all $N(N - 1)/2$ pairs of observations from one an-

other. We carried this out using the Alard & Lupton (1998) code mentioned previously. This procedure produces negative fluxes for some subtractions, but it has the advantage that *every* observation serves as a template for the entire light curve. The details of this procedure are in the Appendix. We have found that this procedure reduces the errors by a factor of about $\sqrt{2}$ (Novicki & Tonry 2000).

There are two unresolved questions after the $N(N - 1)/2$ procedure has been followed. We do not know a flux zero-point, since it has been removed when we difference images, and we need a flux-to-magnitude conversion which incorporates the independent magnitude zero-points established for each image.

The flux zero-point is generally established by late-time observations when there is no remaining supernova flux. This is an improvement over the usual “template” method, because the flux zero-point which comes out of the $N(N - 1)/2$ procedure for the late-time point comes from the average comparison with all the other observations, and the relative fluxes of all the other observations are not dependent solely on the final observation. In some cases where we had several late-time points without supernova flux, we adjusted the flux zero-point to be an average of those points, or to include a first point that was obtained prior to the supernova explosion.

Infrared template images were available only for SN 1999fm and SN 1999fk, so we used standard PSF photometry with the DaoPhot II/Allstar package (Stetson 1987; Stetson & Harris 1988) to measure the *J*-band magnitudes of the SN corrected to the same aperture used for the standard stars. SN 1999fm was not visible in the *J* band. SN 1999fk is near the edge of its host so contamination from the galaxy is negligible. SN 1999fn and SN 1999fv are embedded in their hosts, so contamination may be significant. SN 1999ff is located in a bright ($J \approx 17.5$ mag) elliptical galaxy for which it was essential to subtract the host. We used the IRAF/STSDAS analysis isophote tasks to construct a model of the host, subtracted our model, and then performed PSF photometry on the supernova. We were unable to define a PSF for the Keck observations of SN 1999fn due to the lack of suitable stars in the Keck/NIRC field of view, so we performed aperture photometry in an

TABLE 4—*Continued*

SN name	RA	Dec	V	\pm	R	\pm	I	\pm	Z	\pm
	02:29:05.3	+01:13:46	21.50	0.05	20.46	0.08	18.95	0.04	18.35	0.06
	02:28:42.9	+01:15:31	20.21	0.03	19.92	0.05	19.45	0.06	19.29	0.13
	02:29:02.1	+01:13:14	22.63	0.12	21.49	0.19	19.92	0.10	19.30	0.13
	02:28:42.3	+01:15:16	20.69	0.04	20.32	0.07	19.95	0.10	19.84	0.22

aperture with a radius of one arcsecond.

Tables 5–12 give the derived supernova light curves, and Figure 5 shows the data points and typical fitted light curves.

TABLE 5
OBSERVATIONS OF SN 1999FW

MJD	m	\pm	K	\pm	<i>obs</i>
	V		$K_{V \rightarrow B}$		
51496.25	22.18	0.15	-0.34	0.04	991114_uh
51514.20	23.84	0.86	-0.24	0.03	991202_uh
51529.21	>24.50	...	-0.21	0.04	991217_uh
51875.25	>24.50	...	-0.26	0.05	001127_esi
	R		$K_{R \rightarrow V}$		
51455.27	>24.50	...	-0.20	0.15	991004_12k
51488.15	21.30	0.01	-0.42	0.04	991106_8k
51496.22	21.43	0.02	-0.30	0.06	991114_uh
51514.26	22.40	0.13	-0.15	0.06	991202_uh
51517.21	22.66	0.09	-0.14	0.07	991205_lris
51529.28	23.54	0.21	-0.09	0.07	991217_uh
51875.26	>24.50	...	-0.43	0.09	001127_esi
	I		$K_{I \rightarrow R}$		
51454.28	>24.50	...	-0.53	0.05	991003_12k
51484.34	21.16	0.03	-0.54	0.01	991102_12k
51485.33	21.14	0.04	-0.54	0.01	991103_12k
51496.23	21.34	0.12	-0.52	0.03	991114_uh
51512.31	21.98	0.07	-0.56	0.04	991130_uh
51517.21	22.03	0.03	-0.57	0.04	991205_lris
51875.28	>24.50	...	-0.55	0.10	001127_esi
	Z		$K_{Z \rightarrow I}$		
51496.28	>24.00	...	-0.11	0.07	991114_uh
51517.20	21.92	0.48	-0.08	0.15	991205_lris
51527.22	>24.50	...	0.00	0.16	991216_ufti

TABLE 6
OBSERVATIONS OF SN 1999FH

MJD	m	\pm	K	\pm	obs
	R		$K_{R \rightarrow B}$		
51455.47	>24.50	...	-0.85	0.12	991004_12k
51488.25	22.74	0.02	-0.96	0.07	991105_8k
51496.51	23.02	0.10	-1.02	0.11	991114_uh
51528.23	>24.50	...	-1.44	0.10	991216_uh
51570.29	>24.50	...	-1.32	0.07	000127_lris
51875.30	>24.50	...	-1.28	0.20	001127_esi
	I		$K_{I \rightarrow V}$		
51454.51	>24.50	...	-0.88	0.07	991003_12k
51485.36	22.40	0.07	-0.92	0.02	991103_12k
51496.46	22.41	0.07	-0.91	0.05	991114_uh
51570.27	>24.50	...	-0.94	0.07	000127_lris
51875.29	>24.50	...	-0.95	0.10	001127_esi

TABLE 7
OBSERVATIONS OF SN 1999FF

MJD	m	\pm	K	\pm	<i>obs</i>
	<i>R</i>		$K_{R \rightarrow B}$		
51455.41	>24.50	...	-0.68	0.05	991004_12k
51496.26	22.66	0.04	-0.70	0.02	991114_8k
51496.35	22.72	0.08	-0.70	0.02	991114_uh
51497.48	22.58	0.03	-0.70	0.02	991115_uh
51517.34	24.16	0.22	-0.77	0.03	991205_lris
51529.35	24.39	0.37	-0.82	0.03	991217_uh
51530.28	24.83	0.52	-0.82	0.03	991218_uh
51876.26	>24.50	...	-0.78	0.10	001128_esi
	<i>I</i>		$K_{I \rightarrow V}$		
51454.49	>24.50	...	-0.82	0.05	991003_12k
51484.46	22.86	0.07	-0.84	0.00	991102_12k
51496.28	22.49	0.09	-0.84	0.01	991114_8k
51496.36	22.37	0.12	-0.84	0.01	991114_uh
51497.47	22.27	0.12	-0.84	0.01	991115_uh
51517.32	23.26	0.09	-0.84	0.01	991205_lris
51528.30	23.59	0.20	-0.85	0.01	991216_uh
51876.27	>24.50	...	-0.86	0.05	001128_esi
	<i>Z</i>		$K_{Z \rightarrow R}$		
51496.37	22.85	0.18	-0.79	0.03	991114_uh
51517.37	22.65	0.14	-0.85	0.07	991205_lris
51527.30	23.51	1.19	-0.91	0.06	991216_ufti
51873.22	23.67	1.56	-0.94	0.10	001125_wiyn
	<i>J</i>		$K_{J \rightarrow I}$		
51501.29	22.61	0.10	-0.76	0.03	991119_nirc
51526.31	23.03	0.23	-0.79	0.06	991214_nirc

TABLE 8
OBSERVATIONS OF SN 1999FN

MJD	m	\pm	K	\pm	<i>obs</i>
	<i>R</i>		$K_{R \rightarrow B}$		
51459.59	>24.50	...	-0.75	0.05	991008_12k
51494.30	22.93	0.04	-0.69	0.01	991112_8k
51496.58	22.78	0.06	-0.69	0.01	991114_uh
51497.50	22.71	0.04	-0.69	0.01	991115_uh
51512.29	23.17	0.08	-0.72	0.02	991130_8k
51517.53	23.32	0.12	-0.73	0.02	991205_lris
51518.27	23.49	0.08	-0.73	0.02	991206_8k
51529.44	24.28	0.06	-0.75	0.02	991217_uh
51530.32	24.19	0.03	-0.75	0.02	991218_uh
51545.30	24.92	0.27	-0.77	0.02	000102_8k
51570.36	25.63	0.34	-0.76	0.02	000127_lris
51581.10	>24.50	...	-0.74	0.01	000207_fors
51603.02	>24.50	...	-0.73	0.02	000228_fors
51637.33	>24.50	...	-0.73	0.02	000403_hst
	<i>I</i>		$K_{I \rightarrow V}$		
51459.62	>24.50	...	-0.85	0.02	991008_12k
51485.54	23.26	0.09	-0.86	0.01	991103_12k
51494.32	22.52	0.12	-0.87	0.01	991112_8k
51496.59	22.31	0.10	-0.87	0.01	991114_uh
51497.51	22.37	0.05	-0.87	0.01	991115_uh
51501.34	22.59	0.12	-0.87	0.01	991119_vatt
51512.32	22.55	0.15	-0.85	0.01	991130_8k
51512.49	22.79	0.07	-0.85	0.01	991130_uh
51517.47	23.03	0.08	-0.85	0.01	991205_lris
51518.28	22.97	0.12	-0.85	0.01	991206_8k
51528.41	23.34	0.09	-0.86	0.01	991216_uh
51570.34	>24.50	...	-0.88	0.01	000127_lris
51579.09	>24.50	...	-0.87	0.01	000205_fors
51637.40	>24.50	...	-0.86	0.02	000403_hst
	<i>Z</i>		$K_{Z \rightarrow R}$		
51496.61	22.30	0.56	-0.89	0.03	991114_uh
51497.52	22.02	0.26	-0.88	0.03	991115_uh
51512.54	22.47	0.29	-0.83	0.08	991130_uh
51517.49	22.41	0.05	-0.86	0.09	991205_lris
51518.33	22.75	0.36	-0.87	0.09	991206_8k
51528.42	23.38	0.27	-0.97	0.08	991217_ufti
51530.37	23.31	0.14	-0.98	0.08	991218_uh
51570.24	23.32	0.62	-1.08	0.13	000127_lris
51637.47	>24.50	...	-0.98	0.10	000403_hst
51873.35	>24.50	...	-0.99	0.20	001125_wiyn
	<i>J</i>		$K_{J \rightarrow I}$		

3. SN Ia Analysis

3.1. K-Corrections

K-corrections were calculated using the formulas described by Kim, Goobar, & Perlmutter (1996) and Schmidt et al. (1998). The apparent brightness of a supernova observed in filter j , $m_j(t)$, but with a $z = 0$ absolute magnitude light curve in filter i , $M_i(t)$, is given by

$$m_j(t) = M_i((1+z)t') + 25 + 5 \log \left(\frac{D_L}{\text{Mpc}} \right) + K_{ij}((1+z)t'),$$

where K_{ij} is given by

$$K_{ij} = 2.5 \log \left[(1+z) \frac{\int F_\lambda(\lambda) S_i(\lambda) d\lambda}{\int F_\lambda(\lambda/(1+z)) S_j(\lambda) d\lambda} \right] + \mathcal{Z}_j - \mathcal{Z}_i, \quad (1)$$

for filter energy sensitivity functions S_i and S_j , with zero-points \mathcal{Z}_i and \mathcal{Z}_j , and supernova spectrum F_λ . The luminosity distance, D_L , depends on the cosmological parameters, and is discussed extensively by Schmidt et al. (1998).

For multi-filter light curve shape (MLCS) fitting, K-corrections were calculated in the same manner as for Riess et al. (1998a), as part of the fitting process, using a prescription similar to

that of Nugent et al. (2002). For K-corrections presented in Tables 5–12, we used a set of 135 SN Ia spectra ranging from 14 d before maximum light to 92 d after maximum light. Extending the work of Nugent et al. (2002), before applying the K-correction formulae, the SN Ia spectra of each epoch were matched to the de-reddened U, B, V, R, I color curves of a well-observed set of SN templates, by warping the spectral energy response with a spline containing knots at the effective wavelengths of each filter. In our case we used the compilation of Jha (2002) for SN 1991T, 1994D, 1996X, 1997bp, 1997bq, 1997br, 1998ab, 1998aq, 1998bu, 1998es, 1998V, 1999aa, 1999ac, 1999by, 1999dq, 1999gp. The spectra were corrected for the estimated host extinction in the rest frame, as well as for Galactic extinction in the observer’s frame using the Schlegel et al. (1998) values and the Savage & Mathis (1979) reddening law. The modified spectra were then used to calculate the K-corrections, providing a series of K-correction estimates as a function of SN age, and of SN template type. These values were fitted with a 3-knot spline, and uncertainties estimated from the scatter of allowable templates as dictated by the light-curve fits (in this case, the modified dm15 method of Germany et al. 2001).

Our K-corrections were used to fit the light curve and update the time of maximum light, as well as the allowable supernova template type and host extinction, and the whole process was iterated until convergence (only two iterations were required). Tables 5–12 list the derived K-corrections for each observation along with their uncertainties.

3.2. Light-Curve Fits using MLCS

We fit the photometry of the eight SN Ia shown in Figure 5 using either the MLCS algorithm as described by Riess et al. (1998a) or Riess et al. (2001), depending on the quality of the data.

For SN Ia whose light curve constrains the time of maximum well and whose colors provide sufficient leverage on potential reddening, we fit the photometry using the MLCS algorithm as described by Riess et al. (1998a). This method employs the observed correlation between light-curve shape, luminosity, and colors of SN Ia in the Hubble flow, leading to significant improvements in the precision of distance estimates derived from SN Ia

TABLE 8—*Continued*

MJD	m	\pm	K	\pm	<i>obs</i>
51498.52	22.30	0.20	-0.77	0.02	991116_ufti
51501.36	22.22	0.05	-0.76	0.03	991119_nirc
51526.45	22.86	0.21	-0.79	0.06	991214_nirc
51530.30	22.53	0.39	-0.79	0.07	991218_ufti

TABLE 9
OBSERVATIONS OF SN 1999FJ

MJD	m	\pm	K	\pm	<i>obs</i>
	I		$K_{I \rightarrow B}$		
51454.51	24.90	0.13	-1.02	0.10	991003_12k
51485.36	23.14	0.03	-1.20	0.02	991103_12k
51493.22	23.28	0.05	-1.18	0.03	991111_fors
51496.41	23.70	0.13	-1.17	0.03	991114_uh
51497.12	23.53	0.06	-1.17	0.03	991115_fors
51497.42	23.60	0.15	-1.17	0.03	991115_uh
51512.40	24.45	0.23	-1.18	0.02	991130_uh
51518.06	24.93	0.40	-1.20	0.02	991206_8k
51527.34	25.11	0.50	-1.20	0.02	991215_lris
51538.31	>24.50	...	-1.20	0.03	991226_lris
51808.58	>24.50	...	-1.23	0.03	000921_hst
	Z		$K_{Z \rightarrow V}$		
51493.24	23.37	0.18	-1.07	0.06	991111_fors
51497.14	23.36	0.15	-1.01	0.07	991115_fors
51498.42	23.91	0.29	-0.99	0.08	991116_ufti
51526.07	24.33	0.32	-0.85	0.10	991214_fors
51808.64	>24.50	...	-0.98	0.25	000921_hst

TABLE 10
OBSERVATIONS OF SN 1999FM

MJD	m	\pm	K	\pm	<i>obs</i>
	<i>I</i>		$K_{I \rightarrow B}$		
51459.43	24.44	0.02	-1.35	0.13	991008_12k
51485.47	23.05	0.11	-1.16	0.06	991103_12k
51494.17	23.20	0.06	-1.16	0.09	991112_fors
51496.40	23.22	0.05	-1.15	0.10	991114_lris
51497.17	23.25	0.07	-1.15	0.10	991115_fors
51512.34	23.83	0.15	-1.07	0.10	991130_uh
51517.26	24.32	0.18	-1.02	0.09	991205_lris
51528.19	25.00	0.46	-0.93	0.07	991215_lris
51527.29	24.54	0.06	-0.93	0.07	991215_fors
51538.22	25.19	0.24	-0.89	0.07	991226_lris
51936.22	>24.50	...	-0.93	0.07	010127_lris
	<i>Z</i>		$K_{Z \rightarrow V}$		
51494.19	23.13	0.24	-1.16	0.13	991112_fors
51496.37	23.14	0.11	-1.11	0.14	991114_lris
51497.19	23.30	0.18	-1.09	0.15	991115_fors
51528.02	24.68	0.26	-0.59	0.17	991216_fors
51529.24	24.14	0.32	-0.58	0.18	991218_ufti
51936.24	>24.50	...	-0.75	0.30	010127_lris
	<i>J</i>		$K_{J \rightarrow R}$		
51500.33	22.48	0.18	-1.40	0.06	991118_nirc
51526.28	23.27	0.18	-1.49	0.09	991214_nirc

TABLE 11
OBSERVATIONS OF SN 1999FK

MJD	m	\pm	K	\pm	obs
	I		$K_{I \rightarrow U}$		
51459.43	>24.50	...	-0.62	0.14	991008_12k
51485.47	23.96	0.13	-0.63	0.09	991103_12k
51493.19	23.79	0.12	-0.70	0.07	991111_fors
51496.41	23.45	0.11	-0.73	0.08	991114_lris
51498.37	23.77	0.23	-0.76	0.08	991116_uh
51512.45	23.69	0.17	-0.89	0.07	991130_uh
51517.40	24.02	0.52	-0.92	0.07	991205_lris
51527.18	25.04	0.67	-0.97	0.06	991214_fors
51527.39	24.58	0.29	-0.97	0.06	991215_lris
51804.76	>24.50	...	-1.06	0.10	000917_hst
51964.21	>24.50	...	-1.06	0.15	010224_hst
	Z		$K_{Z \rightarrow B}$		
51496.42	23.07	0.19	-1.42	0.02	991114_lris
51499.38	23.88	0.67	-1.42	0.01	991117_ufti
51501.20	>24.50	...	-1.42	0.00	991119_isaac
51527.02	24.21	0.55	-1.34	0.03	991215_fors
51804.82	>24.50	...	-1.31	0.03	000917_hst
51964.35	>24.50	...	-1.31	0.10	010224_hst
	J		$K_{J \rightarrow V}$		
51501.16	23.26	0.09	-1.49	0.04	991118_isaac

TABLE 12
OBSERVATIONS OF SN 1999FV

MJD	m	\pm	K	\pm	obs
	I		$K_{I \rightarrow U}$		
51454.34	>24.50	...	-0.61	0.13	991003_12k
51485.20	24.17	0.09	-0.59	0.02	991103_12k
	J		$K_{J \rightarrow V}$		
51502.60	23.61	0.20	-1.59	0.05	991120_isaac
51503.53	23.06	0.15	-1.58	0.05	991121_isaac

(Hamuy et al. 1995, 1996b; Riess, Press, & Kirshner 1995, 1996a).

The empirical model for a SN Ia light and color curve is described by four parameters: a date of maximum (t), a luminosity difference (at maximum, Δ), an apparent distance modulus (μ_B), and an extinction (A_B). Due to the redshifts of the supernova host galaxies we first correct the supernova light curves for Galactic extinction (Schlegel et al. 1998), and then determined the host-galaxy extinction.

Although the best extinction estimates and most precise distances are found from SN Ia light curves which have extended temporal and spectral coverage, ideally to ~ 100 d after maximum and 4 or 5 bandpasses (Jha 2002), we only use data within 40 d of maximum light and in rest-frame B and V to match the data which can be sampled at high redshift. This should only compromise our accuracy slightly, however.

For SN 1999fv and SN 1999fh, failure of the *HST* gyros led to data with less than optimal coverage in time. For these two objects we used the snapshot distance method (Riess et al. 1998b) which employs the observed SN Ia spectrum to constrain the age. This approach is significantly less precise than the distance from a well-sampled light curve.

3.3. Light Curve Fits using $\Delta m_{15}(B)$ and dm_{15}

We also use the Δm_{15} method of Phillips et al. (1999) to estimate a distance to each of our SN Ia. Originally, the method characterized the light curve by a parameter tied to the B -band photometry: the decline in magnitudes for a SN Ia in the first 15 days after B -band maximum. With the accumulation of a larger number of well-sampled light curves, it became possible to expand the method so that $\Delta m_{15}(B)$ is determined from the B , V , and I -band light curves. The Phillips et al. method then compares the light curve of a new object with a small number (six) of template light curves.¹⁷

¹⁷The six templates are based on the light curves of seven objects: SN 1991T, 1991bg, 1992A, 1992al, 1992bc, and 1992bo+1993H. The method now compares the light curve of a new object with 6 template light curves (Hamuy et al. 1996b).

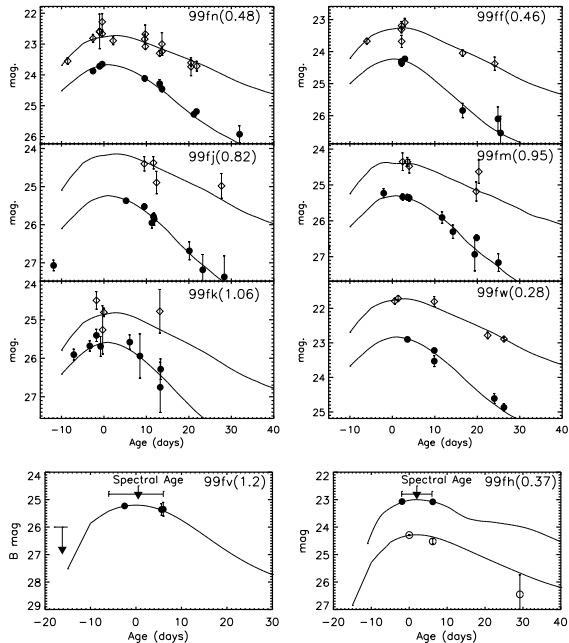


Fig. 5.— MLCS fits to our eight SN Ia. The open diamonds represent K-corrected V -band fits, while the filled-in circles represent K-corrected B -band fits, offset by +1 mag, except for SN 1999fh, which is $V + 1$ and R . SN 1999fo, 1999fi, and 1999fu have no light curves because we could not establish from the spectra that these were indeed SN Ia, so they were not followed. Redshifts are indicated in parentheses.

In contrast to the MLCS method of Riess et al. (1996, 1998a), the Δm_{15} method does not produce a *continuum* of “synthetic” templates. There is a small number of *discrete* templates. The reddening of a SN Ia is determined from the $B - V$ and $V - I$ colors at maximum, and from the $B - V$ colors between 30 and 90 days after V -band maximum. It is assumed that unreddened SN Ia of all decline rates show uniform late-time color curves, as found by Lira (1995). Jha (2002, §3) found that the “Lira law” holds well for the 44 SN Ia studied by him. Only exceptional cases like SN 2000cx seem to deviate greatly from the relation (Li et al. 2001; Candia et al. 2003).

Distances using the modified dm_{15} method are described in detail by Germany (2001). In summary, well-observed SN Ia (approximately 15 ob-

jects) are fitted with a spline in $BVRI$ and assigned a value of $\Delta m_{15}(B)$ based on the method of Phillips (1993) and Phillips et al. (1999). These templates are extended to explosion times using the rise-time measurements of Riess et al. (1999b). SN Ia at $cz > 4000 \text{ km s}^{-1}$ with extinction values from Phillips et al. (1999) are fitted with these templates, with the best-fitting template used to assign these objects a dm_{15} value and maximum-light values B_{max} , V_{max} , R_{max} , and I_{max} . The Hubble velocity then provides an absolute magnitude in each band, from which $M_{B,V,R,I}$ vs dm_{15} relationships are derived. The values found from these relationships are applied to the set of well-observed templates to create a set of absolute magnitude light curves in $BVRI$. To measure the distance to a new supernova, each template is fitted to the data, marginalizing over time of maximum and A_V , to find the distance modulus of the object. The distance is then estimated as the χ^2 -weighted average of each template distance, with the distance uncertainty derived from the union of all templates and distances that have acceptable χ^2 fits.

3.4. Light Curve Fits using BATM

The Bayesian Adapted Template Match (BATM) Method, described by Tonry (2003), uses a set of approximately 20 nearby supernova light curves which are well observed in multiple colors and which span the range of absolute luminosity to predict what they would look like at an arbitrary redshift with an arbitrary host extinction through the actual filters used for observation. Since these SN Ia do not in general have a significant amount of spectrophotometry, the BATM method uses approximately 100 spectral energy distributions (SEDs) of other SN Ia at a variety of SN Ia ages, and warps the SEDs into agreement with the photometry. Given each of the template predictions and a light curve of a new SN Ia, the BATM method then calculates the likelihood distribution as a function of explosion time t_0 , host extinction A_V , and distance d , and marginalizes over t_0 to get a likelihood as a function of A_V and d . This is multiplied by a prior for A_V which is a Gaussian of $\sigma = 0.2$ mag for negative A_V , a Gaussian of $\sigma = 1.0$ for positive A_V , and a delta function at $A_V = 0$ of equal weight. Unfortunately, for these observations (and probably most extant high red-

shift SN Ia distances) there is strong covariance between d and A_V and the choice of prior makes a non-negligible difference in the final estimate for d . The BATM method then combines the probability distributions for all of the template SN Ia and marginalizes over A_V to get a final estimate for the distance.

The BATM method is still undergoing improvement and is not currently “tuned” to minimize scatter of the SN Ia in the Hubble flow. For example, one might expect that certain bandpasses or time spans during a supernova’s light curve might be better predictors of distance (the MLCS method is designed to optimize those choices). The BATM method simply fits all the data available in the observed bandpasses (avoiding the use of K-corrections) without regard for how a set of SN Ia in the nearby Hubble flow behave. As a result, the scatter of the BATM method for these Hubble-flow SN Ia is somewhat larger than that of MLCS (0.22 mag versus 0.18 mag), but it has a different, and perhaps smaller, set of systematic errors.

3.5. Fall 1999 Distances

We list the distance estimates and uncertainties based on our light curves from MLCS, $\Delta m_{15}(B)$, dm_{15} , and BATM in Table 13, along with the empty universe distance modulus corresponding to each redshift. The uncertainties are formal error estimates derived from each method, and we do not attempt here to evaluate whether these estimates are accurate. Below, in Table 15, we do pay attention to the self consistency of the various error estimates. This assumes a nominal value of $H_0 = 65 \text{ km s}^{-1} \text{ Mpc}^{-1}$, though the cosmological inferences do not generally depend on the value of H_0 . The estimates are generally consistent with each other, and we list a “final” distance which is the median of the estimates of each of the four methods. The uncertainty of this “final” distance is taken to be the median of the errors of the contributing methods, because we regard the process of taking a median of different analysis methods not so much sharpening our precision as rejecting non-Gaussian results.

TABLE 13
DISTANCE MODULI ($h = 0.65$)

SN name	MLCS	Δm_{15}	dm15	BATM	Final	$\Omega = 0$
SN 1999fw	40.97 0.31	40.89 0.15	40.80 0.24	40.99 0.42	40.93 0.27	40.82
SN 1999fh	41.77 0.26	41.46 0.47	41.61 0.36	41.52
SN 1999ff	42.38 0.29	42.60 0.22	42.35 0.43	42.61 0.32	42.49 0.30	42.05
SN 1999fn	42.69 0.26	42.36 0.16	41.98 0.40	42.19 0.23	42.27 0.24	42.18
SN 1999fj	44.03 0.22	43.59 0.37	43.76 0.35	43.55 0.43	43.67 0.36	43.62
SN 1999fm	44.18 0.22	44.06 0.23	43.84 0.37	43.77 0.35	43.95 0.29	44.05
SN 1999fk	<44.23 0.30	...	44.26 0.39	44.17 0.36	44.23 0.37	44.36
SN 1999fv	<44.59 0.39	<44.19 0.45	<44.39 0.42	44.74

3.6. Rates

From observations of just three SN Ia at $z \approx 0.4$ Pain et al. (1996) calculated a rate of SN Ia which amounts to $34 \text{ SN Ia yr}^{-1} \text{ deg}^{-2}$, with a 1σ uncertainty of a factor of ~ 2 , for objects found in the range of $21.3 < R < 22.3 \text{ mag}$. A more recent estimate by Pain et al. (2002) is $(1.53 \pm 0.3) \times 10^{-4} h^3 \text{ Mpc}^{-3} \text{ yr}^{-1}$ at a mean redshift of 0.55. Cappellaro et al. (1999) report a nearby rate of SN Ia of $0.36 \pm 0.11 h^2 \text{ SNU}$ (where $1 \text{ SNU} \equiv 10^{10} L_{B_\odot}$ per century) or $(0.79 \pm 0.24) \times 10^{-4} h^3 \text{ Mpc}^{-3} \text{ yr}^{-1}$, using a local luminosity density of $\rho = 2.2 \times 10^8 h L_{B_\odot} \text{ Mpc}^{-3}$. [There is significant uncertainty in the luminosity density, however: Marzke et al. (1998) obtained 1.7×10^8 , and Folkes et al. (1999) found 2.7×10^8 .] Pain et al. (2002) report a very modest increase in the rate of SN Ia with redshift, perhaps tracking the star formation rate which Wilson et al. (2002) estimate as being proportional to $(1+z)^{1.7}$ in a flat universe with $\Omega_M = 0.3$.

Although our Fall 1999 observing was focused on finding candidates for detailed study, it still contains useful information on supernova rates. Two facts help establish rates from this search. First, our observations were very deep in the I band (since we were primarily searching for $z > 1$ SN Ia) and second, because we also sought to find good $z \approx 0.5$ SN Ia for *HST* observations, we obtained spectra for every plausible candidate SN Ia with $z < 0.7$. While we did not obtain light curves for all these candidates, we do know which were Type Ia, and we know their redshifts. This pro-

vides the raw material for a computation of the supernova rate.

At the outset we need to make some reasonable assumption about the underlying luminosity distribution of SN Ia, calculate what fraction of these we would see in our search, and then derive the supernova rate. We assume a luminosity function for SN Ia at maximum which consists of three Gaussians: 64% “normal” SN Ia with mean absolute magnitude $M_B = -19.5 \text{ mag}$ ($h \equiv H_0/(100 \text{ km s}^{-1} \text{ Mpc}^{-1}) = 0.65$) and dispersion $\sigma = 0.45 \text{ mag}$, 20% “SN 1991T” SN Ia with $M_B = -19.8 \text{ mag}$ and dispersion $\sigma = 0.30 \text{ mag}$, and 16% “SN 1991bg” SN Ia with $M_B = -18.0 \text{ mag}$ and dispersion $\sigma = 0.50 \text{ mag}$ (Li et al. 2001a).

Table 14 gives values that a “normal” SN Ia might achieve at maximum, derived from the colors of SN 1995D at maximum and the spectral energy distribution of SN 1994S, with parentheses indicating magnitudes that are less accurate because they involve an extrapolation beyond the data for either of these two objects.

We work in a space of redshift z and m_{max} , where m is the bandpass of interest (I band here). We use the magnitudes of SN 1995D at maximum and the SED of SN 1994S to convert a point in this space to a value for the B -band (rest frame) maximum and therefore a density from our luminosity function. We multiply in a volume factor $dV/dz/d\Omega$ and a factor of $(1+z)^{-1}$ because we are interested in the observer’s rate of observing SN Ia. All of this is done for a flat universe with $(\Omega_M, \Omega_\Lambda)$

TABLE 14
PEAK MAGNITUDES OF NORMAL SN IA

z	B	V	R	I	Z	J
0.05	17.37	17.41	17.36	17.82	17.72	(17.70)
0.10	18.94	18.88	18.80	19.20	19.24	(19.30)
0.20	(20.70)	20.29	20.27	20.36	20.75	(20.96)
0.30	(21.94)	21.08	21.07	20.97	21.28	(21.63)
0.40	(23.07)	21.89	21.62	21.55	21.67	21.97
0.50	(24.06)	(22.59)	22.10	22.01	21.96	22.35
0.60	(24.90)	(23.26)	22.59	22.41	22.37	22.79
0.70	(25.53)	(23.97)	23.06	22.70	22.70	23.06
0.80	(26.00)	(24.75)	(23.54)	22.91	23.01	23.11
0.90	(26.39)	(25.46)	(24.06)	23.12	23.17	23.20
1.00	(26.75)	(26.03)	(24.61)	23.48	23.39	23.25
1.10	(27.08)	(26.45)	(25.14)	23.78	23.50	23.38
1.20	(27.39)	(26.78)	(25.66)	(24.19)	23.72	23.59
1.30	(27.67)	(27.07)	(26.13)	(24.59)	24.11	23.72
1.40	(27.95)	(27.35)	(26.55)	(24.91)	(24.39)	23.94
1.50	(28.20)	(27.60)	(26.93)	(25.36)	(24.70)	24.08
1.60	(28.45)	(27.85)	(27.24)	(25.85)	(25.04)	24.18
1.70	(28.68)	(28.08)	(27.51)	(26.30)	(25.32)	24.32
1.80	(28.90)	(28.30)	(27.75)	(26.77)	(25.72)	24.38

= (0.3 , 0.7). We then convolve the resulting distribution with a dust extinction distribution which approximates the detailed curves of Hatano, Branch, & Deaton (1998): 25% of hosts are “bulge systems” with the probability of a given host A_B given by $f(A_B) \propto 0.02 \delta(A_B) + 10^{-1.25-A_B}$, 75% of hosts are “disk systems” with probability $f(A_B) \propto 0.02 \delta(A_B) + e^{-3.77-A_B^2}$. (The redshifted SEDs tell us how the observed I -band extinction depends on a given host galaxy extinction A_B .) This gives us a distribution for the observed rate of SN Ia as a function of peak apparent I -band magnitude.

However, two complications arise. The “observation time” which must be multiplied into this distribution is a convolution of the search time and the intrinsic time that a given SN Ia is above the detection threshold. Also, our supernova detection threshold is not based only on peak I -band magnitude. We have two search epochs, separated by 31 days, and we have a sensitivity of $I \approx 24$ mag to the flux *difference* between the first and second epochs.

Using the formalism of the BATM method, we place SN 1995D ($\Delta m_{15} = 0.99$, MLCS $\Delta = -0.42$) and SN 1999by ($\Delta m_{15} = 1.93$, MLCS $\Delta = +1.48$) in the z - m_{max} space. Any point in the space between them is assigned a light curve which is the flux interpolation between the redshifted light curves of SN 1995D and SN 1999by. Points which lie brighter or fainter than these two SN Ia are assigned copies of one or the other light curves which are simply scaled brighter or fainter to match the desired peak brightness. Given a light curve, we calculate the visibility time for each point in the (z, m_I) diagram, using a 31 d lag time and a sensitivity of $I < 24$ mag. (Our actual probability of detecting a supernova rolls off gradually at fainter magnitudes, but we had S/N ≈ 10 at $I < 24$ mag and we ignored candidates which we thought would peak at $I > 24$ mag, hence the approximation of a step at $I = 24$ mag.)

The resulting difference light curve is identical to the actual light curve when the explosion occurs after the first epoch, but for explosions that erupted earlier than the first epoch, taking the difference between our two observation epochs decreases the difference and can be negative. Low-luminosity SN Ia with rapid rise and declines would be visible for a shorter time than higher-

luminosity SN Ia with their slowly declining light curves, so they are less likely to be found. For the purpose of calculating rates, the total time that a supernova could be detected is a convolution of the time that the difference flux from the supernova explosion exceeds the sensitivity limit and the search time (a delta function in this case).

Figure 6 shows contours of predicted rates (number per observer’s month per square degree per magnitude per unit redshift). We plot our eight SN Ia as well as three other SN Ia which we did not follow. Without light curves for these three, we can only show the discovery (difference) magnitude which is an upper limit to the peak I band magnitude that was eventually reached.

The normalization of Figure 6 is adjusted to bring the cumulative distribution as a function of z into agreement with our observations. Figure 7 integrates the lower panel of Figure 6 over magnitude and then assembles the cumulative predicted number of SN Ia as a function of redshift. We compare this with the number observed to normalize the model. Our sensitivity limit was approximately $I < 24$ mag, and the time between our first and second search epochs was 31 d. Our total area surveyed (including the cloudy second epoch) was 3.0 deg², of which we lost about 15% due to chip edges, bad columns, stars, etc., so our effective search area was about 2.5 deg². Subsequent tests of our search technique using synthetic SN Ia injected into the images indicate that we miss very few objects down to the quoted sensitivity limit.

Uncertainties in the searched area, effective time sampling, and modeling of supernova properties amount to perhaps 10–20%, and a similar uncertainty is the fraction of objects which we detected photometrically but for which we did not obtain spectroscopy. Since our goal was to find suitable targets for *HST* studies and to find supernovae at $z \approx 0.5$, we were not complete in our spectroscopic follow-up. Subjective factors go into the decision of which objects to follow. For example, if we find a candidate at $I = 23.5$ mag, but it appears to be in a galaxy at $z \approx 0.3$, we might very well choose not to get a spectrum, reasoning that “the supernova is well past maximum” or “it might be a type II” or “it might be highly extinguished, or a SN 1991bg-type”. Spectroscopic resources are *so* valuable that our first priority, to obtain targets, often outweighs our desire to con-

trol systematics. The factors in these decisions change with redshift of the supernova: we believe we were complete in our search to $z < 0.6$ (even though we did not follow three SN Ia photometrically), but we were definitely not complete for more distant and fainter SN Ia. The lower panel of Figure 6 shows that the counts of SN Ia to a redshift of $z < 0.6$ are not very sensitive to our estimate of our completeness limit.

Figure 7 shows the comparison between this model cumulative distribution and the observed rates for our Fall 1999 campaign. The Poisson statistics of the 8 SN Ia counted with $z < 0.6$ are still the largest source of uncertainty, and we estimate our overall normalization is accurate to about 35%. The slope agreement between the observations and the model in Figure 7 reassures us that our model is reasonably accurate.

These model predictions, which we calculate for comparison with the observations, include complicated factors for visibility within a time window and sensitivity limit, convolution with dust extinction, time dilation factors of $(1 + z)$, and volume factors of $dV/dz/d\Omega$. The fundamental normalization that goes into the calculation and that brings the model into agreement with the observations shown in Figure 7 amounts to 40,000 SN Ia of all sub-types per Gpc³ per (rest frame) year for the Hubble constant used above ($H_0 = 65 \text{ km s}^{-1} \text{ Mpc}^{-1}$) for the SN Ia luminosity function. Put in more sensible units, this is a rate of $r = (1.4 \pm 0.5) \times 10^{-4} h^3 \text{ Mpc}^{-3} \text{ yr}^{-1}$ SN Ia at a mean redshift of $z = 0.46$. So the observed rate of SN Ia from a shell at redshift z is

$$dN = r d\Omega (dV/dz/d\Omega) (1 + z)^{-1} \Delta t,$$

where Δt has to be integrated over the luminosity function of SN Ia and the search parameters. These rates are in excellent agreement with those of Pain et al. (2002), and are not inconsistent with the local rates from Cappellaro et al. (1999), particularly given the uncertainty in the local luminosity density.

Although we were not complete in our counts of SN Ia at $z \approx 1$, we do not believe it is possible that the rate of SN Ia closely tracks the star formation rate (SFR). Application of the SFR from Wilson et al. (2002) would suggest that the rate at $z \approx 1.1$ should be three times as great as occurs locally and nearly twice as great as the rate

at $z = 0.46$. Our model illustrated in Figure 7, if altered from constant rate per comoving volume to one which tracks the SFR of Wilson et al. (2002), would predict 16 SN Ia deg⁻² in our search instead of 6.5 (we discovered 4). It is our impression that the constant rate per volume is closer to the truth — SN Ia at $m_I = 24$ mag are simply not that common. Obviously, SN Ia explosions lag star formation by some unknown time distribution. This suggests the lag must span a substantial fraction of the time between the peak of star formation and the time when a supernova observed at $z \sim 1$ explodes, which is about 2 Gyr. As pointed out by Pain et al. (2002), we should obtain better constraints on any increase in SN Ia rate at $z > 1$ from ongoing search campaigns.

3.7. A Homogeneous Set of SN Ia Distances

As standardizable candles, SN Ia have played an extremely important role in recent years. However, observations of SN Ia are so difficult and resource-intensive that the results have appeared in a large number of papers, using a variety of distance zero-points, photometric calibrations, etc. We have therefore undertaken to draw all the results available to us together into a single table with a common calibration.

The most recent data apart from the observations presented here are the results from the campaigns of the HZT in 1997 (Leibundgut et al. 2003), 1998 (Suntzeff et al. 2003), 1999 (Clocchiatti et al. 2003), and 2000 (Jha et al. 2003b).

In the 1997 data, there are four spectroscopically classified SN Ia (SN 1997as, 1997bb, 1997bh, and 1997bj) and one object in an elliptical galaxy (SN 1997bd) at redshifts in the range 0.33 to 0.67. The redshifts are all from narrow emission lines associated with the host galaxies, and on the prominent Ca II H&K absorption in the elliptical galaxy. The supernova spectrum in all cases yielded an age concordant with the light curves. Light curves in the R and I filters have been established for all objects. The campaign in 1997 made use of ground-based telescopes only. The distance moduli, colors, and absorptions are given in Table 15.

From our 1998 campaign, Suntzeff et al. (2003) report photometry and spectroscopy of six SN Ia: 1998I, 1998J, 1998M, 1998ac, 1998ai, and 1998aj.

A seventh object (SN 1998ah) was only observed spectroscopically. These seven objects range in redshift from 0.43 to 0.887. One of the significant results of the 1998 and 1999 (see below) campaigns was the comparison of the photometry of the SN Ia and nearby field stars from ground-based and *HST* observations: we found that the zero-points of the photometry agree to within 0.02 mag, which is reassuring. Since the highest-weighted points in light curves of high- z supernovae are usually the *HST* data, owing to their smaller statistical uncertainties, we naturally wanted to compare photometry obtained on the ground and in space. Because the evidence from supernova observations for a non-zero cosmological constant hinges on a systematic faintness of SN Ia at $z \approx 0.5$ by 0.22 mag, we are now quite confident that the systematic faintness of supernovae at such redshifts is *not* due to a zero-point error between space-based and ground-based light curves.

In the Spring 1999 campaign, Clocchiatti et al. (2003) find five spectroscopically classified SN Ia: SN 1999M, 1999N, 1999Q, 1999S, and 1999U. All of them were followed up from ground-based observatories and two of them, SN 1999Q and SN 1999U, were observed with *HST*. We report in Table 15 the distance moduli to the latter two based on the *HST* photometry. The redshift of SN 1999U was obtained from emission lines in the parent galaxy, and that of SN 1999Q from cross correlating its spectrum with nearby SN Ia close to maximum light.

The 2000 campaign was intended primarily to investigate the possibility that gray dust was causing the dimming we attribute to cosmology. Jha et al. (2003b) present photometry over a very wide wavelength range. There are six SN Ia at a redshift of ~ 0.5 whose distances we include in Table 15: SN 2000dz, 2000ea, 2000ec, 2000ee, 2000eg, and 2000eh.

In addition to these observing campaigns of the HZT, we also drew from the literature all SN Ia results we could find. In cases where we had access to the observational data and photometry we re-computed fits to the distance and extinction using the MLCS98 method of Riess et al. (1998a), the MLCS2k2 improvement of Jha et al. (2003c), and the dm15 and BATM methods described above. In other cases, such as the Supernova Cosmology Project (SCP; Perlmutter et al. 1999), which has

not published their photometry, we took their published distances, extinctions, and uncertainties at face value. One might expect that applying multiple fitting techniques as we have done helps decrease errors in the derived distances. The SCP-only results appear to have at least a factor of 2 more scatter with respect to a cosmological fit than our data. This could be due to the quality of the underlying photometry, or to a less varied approach to the analysis.

Assembling all of these results from the literature and performing new fits when possible, we obtain long lists of SN Ia results for each method which are internally self-consistent, but which have unknown offsets with respect to one another because of differing and inconsistent assumptions about Hubble constants and zero-points. We also have one more distance measure, derived from the redshift of the SN Ia in the “Hubble flow” (defined as $0.01 < z < 0.1$) and the luminosity distance for an empty universe:

$$D_L = \frac{cz}{H_0} \left(1 + \frac{z}{2}\right). \quad (2)$$

All of the methods overlap for many SN Ia, particularly the Calán-Tololo sample (Hamuy et al. 1996a), with even the SCP results having 17 or 18 overlaps with the rest, and the other methods having 52–108 overlaps. In order to determine the zero-point offsets we compute the median difference between all pairs of methods, forming an antisymmetric matrix, and then fit this matrix as differences between components of a zero-point vector. The residuals are quite well behaved, with the worst agreement between SCP and MLCS98 at 0.07 mag, and the rest 0.02 mag or better. We put all the methods on the Hubble flow zero-point, i.e., distance in Mpc multiplied by H_0 .

It is beyond the scope of this paper to analyze and optimize the combination of the published data. We do note that there actually does appear to be a modest improvement in accuracy (judged by scatter with respect to the cosmological line) by combining different fitting methods. Nevertheless, we are concerned about the susceptibility to bias which might creep in if we optimize scatter with respect to the parameters we seek to measure, so we choose to use medians, a simple and robust combination scheme. Our “best distance” for each SN Ia is just the median of all the

distances of all the different methods (excepting redshift-based luminosity distance!). The best distances for the Fall 1999 data presented here differ slightly from those in Table 13 because we did not have Δm_{15} distances for more than the Fall 1999 data and we thought that for the sake of consistency we should treat the Fall 1999 data in the same way as the other SN Ia for which we have observations. The scatter between the distances in Table 13 and Table 15 is 0.08 mag.

Obtaining accurate uncertainties is somewhat more complicated. The scatter of any method’s results around any cosmological may not match the error estimates. We therefore examine this scatter for each method, prune at 3σ , and multiply the error estimates for each method by a factor to bring them into agreement with the scatter. This appears to be a more realistic adjustment than adding a “cosmic scatter” in quadrature (which we already do anyway when called for). We then obtain a final error estimate as the median of all of the contributing methods’ errors diminished by the $1/4$ power of the number of contributors (a factor empirically derived by examining scatter around cosmological models). As above, we believe the covariance between the different methods applied to the same data is such that we are getting only a minimal improvement in accuracy by taking a median, but we hope that we are thereby “Gaussianizing” the distribution. The final list comprises 230 SN Ia.

We will use this list below for determining cosmological parameters, and although we will not repeat the data we found in the literature, we thought it important to publish the actual distances which are being used for calculation of cosmological parameters as well as other relevant information which may be of use to others. In Table 15 we list the supernova name, its Galactic coordinates, host, and literature reference. We give the redshift as $\log(cz)$ and the luminosity distance and error in the same units, i.e., we do *not* want to use uncertain units of Mpc when we know the Hubble flow zero-point so exquisitely well. The median of the estimates for host-galaxy extinction in the rest-frame V band follows, where we have used a standard Cardelli, Clayton, & Mathis (1989) extinction law to bring estimates in different bandpasses to V . Finally we identify the methods which contributed to the median: MLCS98 =

R, SCP/stretch = P, MLCS2k2 = J, dm15 = S, and BATM = T.

TABLE 15
SNIa SUMMARY

SN	l^{II}	b^{II}	z	Host	Ref. ^a	$\log(cz)$	$\langle \log(dH_0) \rangle$	\pm	$\langle A_V \rangle$	Contrib
sn72E	314.840	30.080	0.0023	N5253	16	2.839	2.399	0.033	0.10	RT
sn80N	240.161	-56.689	0.0056	N1316	9	3.225	3.140	0.043	0.21	RT
sn81B	292.970	64.743	0.0072	N4536	2	3.334	3.077	0.041	0.25	RT
sn81D	240.161	-56.689	0.0056	N1316	9	3.225	3.044	0.055	0.31	JT
sn86G	309.543	19.401	0.0027	N5128	26	2.908	2.440	0.035	0.49	RT
sn88U	8.737	-81.227	0.3100	Anon	24	4.968	5.096	0.072	0.10	RT
sn89B	241.991	64.403	0.0036	N3627	37	3.033	2.844	0.030	0.74	RST
sn90N	294.369	75.987	0.0044	N4639	21	3.120	3.204	0.035	0.30	RST
sn90O	37.654	28.360	0.0307	M+034403	10	3.964	3.977	0.025	0.09	RPJST
sn90T	341.503	-31.526	0.0400	P63925	10	4.079	4.101	0.042	0.25	RJT
sn90Y	232.645	-53.854	0.0390	Anon	10	4.068	3.985	0.039	0.54	RJT
sn90af	330.823	-42.235	0.0500	Anon	10	4.176	4.149	0.026	0.06	RPJST
sn91M	30.392	45.900	0.0076	I1151	5	3.358	3.397	0.030	0.00	R
sn91S	214.061	57.426	0.0560	U05691	10	4.225	4.283	0.042	0.11	RJT
sn91T	292.609	65.191	0.0070	N4527	21	3.322	2.961	0.028	0.50	RST
sn91U	311.824	36.212	0.0331	I4232	10	3.997	3.938	0.032	0.47	RJST
sn91ag	342.556	-31.639	0.0141	I4919	10	3.626	3.626	0.025	0.11	RJST
sn91bg	278.227	74.464	0.0042	N4374	4	3.100	3.064	0.035	0.02	RT
sn92A	235.896	-54.059	0.0058	N1380	33	3.240	3.124	0.023	0.08	RST
sn92G	184.623	59.851	0.0062	N3294	5	3.269	3.286	0.030	0.29	RT
sn92J	263.540	23.545	0.0460	Anon	10	4.140	4.099	0.033	0.27	RJST
sn92K	306.275	16.309	0.0112	E269-57	10	3.526	3.432	0.036	0.56	RJST
sn92P	295.617	73.110	0.0265	I3690	10	3.900	3.939	0.027	0.13	RPJST
sn92ae	332.706	-41.988	0.0750	Anon	10	4.352	4.359	0.026	0.14	RPJST
sn92ag	312.490	38.386	0.0262	E508-67	10	3.895	3.864	0.031	0.49	RPJST
sn92al	347.337	-38.490	0.0141	E234-69	10	3.626	3.636	0.026	0.06	RPJT
sn92aq	1.776	-65.315	0.1010	Anon	10	4.481	4.513	0.027	0.04	RPJST
sn92au	319.112	-65.883	0.0610	Anon	10	4.262	4.252	0.030	0.13	RJST
sn92bc	245.694	-59.635	0.0186	E300-09	10	3.746	3.777	0.021	0.03	RPJST
sn92bg	274.611	-18.346	0.0360	Anon	10	4.033	4.036	0.030	0.24	RPJST
sn92bh	267.849	-37.328	0.0450	Anon	10	4.130	4.191	0.026	0.33	RPJST
sn92bi	63.264	47.239	0.4580	Anon	25	5.138	5.301	0.095	...	P
sn92bk	265.036	-48.918	0.0580	E156-08	10	4.240	4.222	0.025	0.11	RJST
sn92bl	344.129	-63.925	0.0430	E291-11	10	4.110	4.095	0.022	0.06	RPJST
sn92bo	261.995	-80.348	0.0178	E352-57	10	3.727	3.745	0.021	0.04	RPJST
sn92bp	208.832	-51.096	0.0790	Anon	10	4.374	4.336	0.026	0.05	RPJST
sn92br	288.014	-59.428	0.0880	Anon	10	4.421	4.441	0.027	0.07	RPJST
sn92bs	240.028	-55.345	0.0630	Anon	10	4.276	4.327	0.026	0.19	RPJST
sn93B	273.324	20.460	0.0710	Anon	10	4.328	4.345	0.026	0.32	RPJST
sn93H	318.223	30.336	0.0251	E445-66	10	3.876	3.845	0.026	0.32	RJST
sn93O	312.414	28.926	0.0520	Anon	10	4.193	4.231	0.026	0.08	RPJST
sn93ac	149.707	17.212	0.0490	P17787	30	4.167	4.206	0.043	0.49	RJST

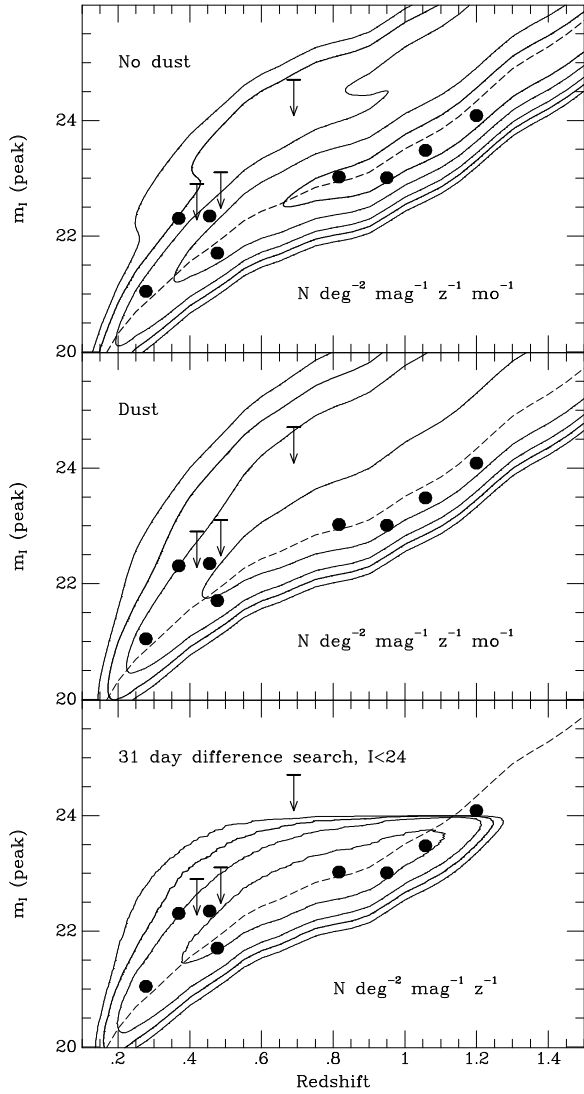


Fig. 6.— Distribution of SN Ia occurrence as a function of peak I -band magnitude and redshift. Contours of predicted rates are drawn with heavy curves at 1 and 10, and light curves at intervening intervals of 2 and 5. The ridge line of an unreddened “normal” SN Ia is drawn as a dashed line. The upper panel shows the distribution based on the SN Ia luminosity function if there were no reddening; the middle panel shows the effect of convolving with the model extinction distribution; and the bottom panel shows the expected distribution for our search parameters.

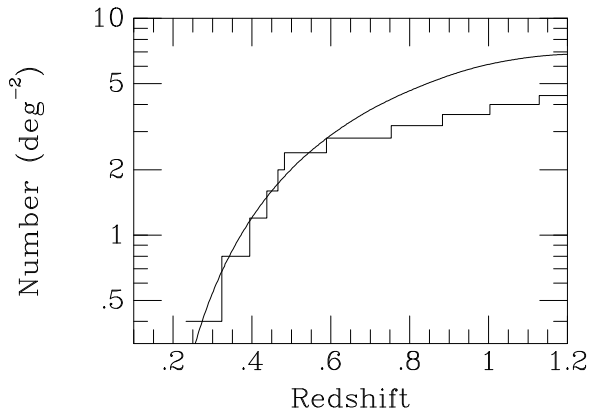


Fig. 7.— Cumulative number of SN Ia discovery is shown as a function of redshift. The histogram is the observed SN Ia; the curve is the prediction of what we should have seen given a flux limit of $I < 24$ mag and a 31 d difference search. We think that our search is nearly complete for $z \leq 0.6$, but do *not* claim completeness for $z > 0.6$, because of the necessity to pick a subset for spectroscopy.

TABLE 15—*Continued*

SN	l^I	b^I	z	Host	Ref. ^a	$\log(cz)$	$\langle \log(dH_0) \rangle$	\pm	$\langle A_V \rangle$	Contrib
sn93ae	144.629	-63.220	0.0180	U01071	30	3.732	3.684	0.024	0.17	RJST
sn93ag	268.435	15.929	0.0500	Anon	10	4.176	4.209	0.026	0.26	RPJST
sn93ah	25.876	-76.771	0.0286	E471-27	10	3.933	3.933	0.032	0.18	RJST
sn94B	208.140	26.669	0.0900	Anon	29	4.431	4.507	0.030	0.00	R
sn94C	174.632	29.922	0.0510	M+081523	29	4.184	4.139	0.036	0.00	R
sn94D	290.151	70.140	0.0027	N4526	27	2.908	3.003	0.026	0.06	RT
sn94F	258.613	68.127	0.3540	Anon	25	5.026	5.155	0.075	...	P
sn94G	162.893	52.779	0.4250	Anon	25	5.105	5.105	0.100	...	P
sn94H	173.057	-53.517	0.3740	Anon	25	5.050	5.023	0.060	...	P
sn94M	291.687	63.033	0.0244	N4493	30	3.864	3.835	0.026	0.40	RJST
sn94Q	64.384	39.680	0.0290	P59076	30	3.939	3.955	0.026	0.26	RJST
sn94S	187.377	85.142	0.0161	N4495	30	3.684	3.693	0.024	0.04	RJST
sn94T	318.017	59.838	0.0360	P46640	30	4.033	4.014	0.025	0.17	RJST
sn94U	308.732	54.772	0.0056	N4948	29	3.225	3.149	0.030	0.00	R
sn94ae	225.342	59.665	0.0054	N3370	30	3.209	3.295	0.028	0.29	RST
sn94al	163.157	-34.816	0.4200	Anon	25	5.100	5.189	0.064	...	P
sn94am	173.104	-53.563	0.3720	Anon	25	5.047	5.131	0.057	...	P
sn94an	69.409	-49.082	0.3780	Anon	25	5.054	5.195	0.081	...	P
sn95D	230.027	39.659	0.0077	N2962	30	3.363	3.373	0.024	0.08	RST
sn95E	141.994	30.262	0.0116	N2441	30	3.541	3.559	0.034	2.18	RS
sn95K	259.953	43.327	0.4780	Anon	28	5.156	5.284	0.038	0.02	RT
sn95M	246.716	28.833	0.0530	Anon	29	4.201	4.243	0.044	0.10	RT
sn95ac	58.694	-55.049	0.0490	Anon	30	4.167	4.160	0.028	0.24	RJST
sn95ae	76.817	-56.240	0.0680	Anon	29	4.309	4.315	0.086	0.00	R
sn95ak	169.658	-48.982	0.0219	I1844	30	3.817	3.772	0.033	0.55	RJST
sn95al	192.179	50.835	0.0060	N3021	30	3.255	3.328	0.026	0.31	RST
sn95ao	178.196	-50.515	0.3000	Anon	29	4.954	4.957	0.156	0.00	R
sn95ap	179.359	-46.149	0.2300	Anon	29	4.839	4.893	0.120	0.00	R
sn95aq	113.341	-54.599	0.4530	Anon	25	5.133	5.313	0.064	...	P
sn95ar	127.657	-58.471	0.4650	Anon	25	5.144	5.345	0.070	...	P
sn95as	127.757	-58.339	0.4980	Anon	25	5.174	5.421	0.064	...	P
sn95at	129.274	-58.142	0.6550	Anon	25	5.293	5.333	0.058	...	P
sn95aw	165.472	-54.078	0.4000	Anon	25	5.079	5.151	0.056	...	P
sn95ax	166.056	-53.909	0.6150	Anon	25	5.266	5.317	0.064	...	P
sn95ay	176.870	-48.453	0.4800	Anon	25	5.158	5.271	0.062	...	P
sn95az	202.114	-31.504	0.4500	Anon	25	5.130	5.181	0.061	...	P
sn95ba	215.987	22.984	0.3880	Anon	25	5.066	5.209	0.057	...	P
sn95bd	187.111	-21.660	0.0152	U03151	30	3.659	3.648	0.029	0.94	RJST
sn96C	99.624	65.036	0.0276	M+082547	30	3.918	3.989	0.026	0.32	RJST
sn96E	253.120	34.311	0.4250	Anon	28	5.105	5.156	0.066	0.15	RT
sn96H	290.752	62.242	0.6200	Anon	28	5.269	5.397	0.043	0.04	RT
sn96I	276.852	60.008	0.5700	Anon	28	5.233	5.356	0.053	0.07	RT

TABLE 15—*Continued*

SN	l^I	b^I	z	Host	Ref. ^a	$\log(cz)$	$\langle \log(dH_0) \rangle$	\pm	$\langle A_V \rangle$	Contrib
sn96J	253.221	34.301	0.3000	Anon	28	4.954	5.010	0.064	0.26	RT
sn96K	224.381	20.459	0.3800	Anon	28	5.057	5.183	0.049	0.03	RT
sn96R	259.070	54.356	0.1510	Anon	29	4.656	4.621	0.104	0.00	R
sn96T	247.589	37.000	0.2410	Anon	29	4.859	4.941	0.112	0.00	R
sn96U	259.357	68.005	0.4300	Anon	28	5.110	5.288	0.054	0.05	RT
sn96V	257.577	57.537	0.0250	N3644	29	3.875	3.871	0.057	0.00	R
sn96X	310.232	35.649	0.0078	N5061	30	3.369	3.266	0.024	0.08	RST
sn96Z	253.609	22.559	0.0087	N2935	30	3.416	3.387	0.036	0.55	RST
sn96ab	43.159	56.932	0.1240	Anon	30	4.570	4.621	0.032	0.05	RJST
sn96af	319.640	-43.222	0.1000	Anon	7	4.477	4.428	0.040	0.00	S
sn96ag	356.386	-49.535	0.1400	Anon	8	4.623	4.680	0.045	0.00	S
sn96ai	101.583	79.246	0.0041	N5005	30	3.090	3.109	0.121	4.08	RS
sn96am	355.950	-49.361	0.0650	A3809	8	4.290	4.356	0.043	0.32	S
sn96ao	265.439	-51.259	0.0580	A3128	8	4.240	4.240	0.067	0.52	S
sn96bk	111.255	54.881	0.0072	N5308	30	3.334	3.298	0.041	0.81	RST
sn96bl	116.992	-51.302	0.0348	Anon	30	4.018	4.033	0.031	0.28	RJST
sn96bo	144.460	-48.956	0.0165	N0673	30	3.694	3.653	0.032	0.86	RST
sn96bv	157.337	17.972	0.0167	U03432	30	3.700	3.663	0.036	0.73	RJST
sn96bx	263.413	-46.747	0.0580	Anon	8	4.240	4.256	0.130	0.36	S
sn96cf	250.449	50.009	0.5700	Anon	25	5.233	5.333	0.060	...	P
sn96cg	220.767	22.154	0.4900	Anon	25	5.167	5.299	0.057	...	P
sn96ci	333.110	62.084	0.4950	Anon	25	5.171	5.245	0.056	...	P
sn96ck	301.409	62.096	0.6560	Anon	25	5.294	5.393	0.068	...	P
sn96cl	256.574	48.668	0.8270	Anon	25	5.394	5.609	0.108	...	P
sn96cm	10.891	46.743	0.4500	Anon	25	5.130	5.313	0.061	...	P
sn96cn	334.314	61.810	0.4300	Anon	25	5.110	5.305	0.060	...	P
sn97E	140.201	25.814	0.0132	N2258	11	3.597	3.624	0.024	0.29	RJST
sn97F	204.472	-28.455	0.5800	Anon	25	5.240	5.371	0.061	...	P
sn97G	202.331	-26.508	0.7620	Anon	25	5.359	5.573	0.107	...	P
sn97H	202.374	-26.214	0.5260	Anon	25	5.198	5.309	0.057	...	P
sn97I	202.366	-26.207	0.1720	Anon	25	4.712	4.713	0.055	...	P
sn97J	209.921	15.374	0.6190	Anon	25	5.269	5.439	0.068	...	P
sn97K	216.354	16.082	0.5920	Anon	25	5.249	5.563	0.081	...	P
sn97L	220.026	21.876	0.5500	Anon	25	5.217	5.381	0.064	...	P
sn97N	220.656	22.099	0.1800	Anon	25	4.732	4.765	0.054	...	P
sn97O	220.066	22.446	0.3740	Anon	25	5.050	5.383	0.062	...	P
sn97P	256.583	48.254	0.4720	Anon	25	5.151	5.301	0.056	...	P
sn97Q	256.878	48.379	0.4300	Anon	25	5.110	5.193	0.055	...	P
sn97R	256.950	48.501	0.6570	Anon	25	5.294	5.445	0.061	...	P
sn97S	256.960	48.704	0.6120	Anon	25	5.264	5.417	0.058	...	P
sn97Y	124.772	62.369	0.0166	N4675	11	3.697	3.730	0.039	0.19	JT
sn97ac	220.010	22.485	0.3200	Anon	25	4.982	5.051	0.055	...	P

TABLE 15—*Continued*

SN	l^I	b^I	z	Host	Ref. ^a	$\log(cz)$	$\langle \log(dH_0) \rangle$	\pm	$\langle A_V \rangle$	Contrib
sn97af	220.026	22.419	0.5790	Anon	25	5.239	5.375	0.060	...	P
sn97ai	249.958	50.362	0.4500	Anon	25	5.130	5.245	0.070	...	P
sn97aj	256.605	48.217	0.5810	Anon	25	5.241	5.297	0.060	...	P
sn97am	256.340	49.057	0.4160	Anon	25	5.096	5.193	0.057	...	P
sn97ap	333.646	61.901	0.8290	Anon	25	5.395	5.543	0.060	...	P
sn97as	224.726	20.115	0.5080	Anon	17	5.183	5.158	0.049	0.44	RST
sn97aw	239.440	47.883	0.4400	Anon	17	5.120	5.355	0.050	0.36	RS
sn97bb	290.721	62.492	0.5180	Anon	17	5.191	5.356	0.049	0.04	RST
sn97bd	296.961	62.650	0.6710	Anon	17	5.304	5.200	0.065	0.99	ST
sn97bh	330.050	59.713	0.4200	Anon	17	5.100	5.242	0.049	0.33	RST
sn97bj	248.760	48.844	0.3340	Anon	17	5.001	5.070	0.051	0.20	ST
sn97bp	301.157	51.213	0.0095	N4680	11	3.455	3.416	0.025	0.44	RJST
sn97bq	136.293	39.485	0.0096	N3147	11	3.459	3.484	0.023	0.42	JST
sn97br	311.841	40.328	0.0080	E576-40	11:18	3.380	3.282	0.026	0.47	JT
sn97by	312.690	34.865	0.0450	A1736	8	4.130	4.084	0.039	0.16	S
sn97bz	259.751	56.407	0.0313	Anon	8	3.972	4.060	0.116	3.11	S
sn97ce	69.240	36.620	0.4400	Anon	28	5.120	5.228	0.041	0.03	RT
sn97cj	125.800	54.608	0.5000	Anon	28	5.176	5.323	0.047	0.05	RT
sn97ck	57.602	38.452	0.9700	Anon	28	5.464	5.638	0.075	0.17	RT
sn97cn	9.137	69.506	0.0175	N5490	11:36	3.720	3.730	0.026	0.06	JT
sn97cp	336.902	-45.466	0.1600	Anon	8	4.681	4.792	0.098	0.45	S
sn97cu	265.042	-51.213	0.0620	A3128	8	4.269	4.240	0.045	0.00	S
sn97cw	113.095	-49.487	0.0164	N0105	11	3.692	3.674	0.028	1.04	JST
sn97dg	103.616	-33.984	0.0297	Anon	11	3.950	4.033	0.029	0.25	JST
sn97do	171.001	25.269	0.0104	U03845	11	3.494	3.545	0.028	0.32	JST
sn97dr	253.245	-55.861	0.0750	A3112	8	4.352	4.296	0.039	0.00	S
sn97dt	87.564	-39.122	0.0061	N7448	11	3.262	3.375	0.043	0.46	JT
sn97fb	242.377	-37.317	0.0530	A3301	8	4.201	4.254	0.045	0.71	S
sn97fc	242.691	-37.596	0.0540	A3301	8	4.209	4.230	0.039	0.10	S
sn97fd	264.995	-49.215	0.1900	Anon	8	4.756	4.888	0.065	0.00	S
sn97ff	125.906	54.831	1.7550	Anon	32	5.721	5.905	0.083	0.00	R
sn98D	63.777	72.905	0.0132	N5440	11	3.597	3.605	0.069	0.20	J
sn98I	216.646	18.718	0.8870	Anon	34	5.425	5.575	0.053	0.25	JST
sn98J	238.498	32.106	0.8330	Anon	34	5.397	5.615	0.052	0.26	JST
sn98M	260.707	60.423	0.6300	Anon	34	5.276	5.396	0.045	0.28	RST
sn98V	43.942	13.346	0.0170	N6627	11	3.707	3.686	0.028	0.31	JST
sn98ab	124.861	75.194	0.0278	N4704	11	3.921	3.876	0.025	0.59	JST
sn98ac	239.012	31.832	0.4670	Anon	34	5.146	5.260	0.043	0.27	RST
sn98aj	238.163	31.312	0.8600	Anon	34	5.411	5.698	0.070	0.20	ST
sn98aq	138.837	60.269	0.0037	N3982	1	3.045	3.181	0.023	0.06	RST
sn98bp	43.643	20.481	0.0104	N6495	11	3.494	3.475	0.029	0.42	RJST
sn98br	6.580	50.757	0.0810	A2029	8	4.385	4.442	0.063	0.39	S

TABLE 15—*Continued*

SN	l^I	b^I	z	Host	Ref. ^a	$\log(cz)$	$\langle \log(dH_0) \rangle$	\pm	$\langle A_V \rangle$	Contrib
sn98bu	234.413	57.020	0.0043	N3368	12	3.110	2.912	0.028	1.03	RST
sn98cm	332.822	62.779	0.0800	A1780	8	4.380	4.398	0.059	0.36	S
sn98co	41.520	-44.941	0.0171	N7131	11	3.710	3.729	0.046	0.28	JT
sn98cs	65.238	43.339	0.0327	U10432	11	3.991	3.956	0.037	0.03	RT
sn98de	122.031	-35.241	0.0157	N0252	11:23	3.673	3.727	0.024	0.68	JST
sn98dh	82.828	-50.644	0.0076	N7541	11	3.358	3.403	0.034	0.50	ST
sn98dk	102.856	-62.161	0.0120	U00139	11	3.556	3.571	0.028	0.80	JST
sn98dm	145.975	-67.406	0.0054	M+010444	11	3.209	3.498	0.028	1.06	ST
sn98do	135.234	-61.849	0.0920	Anon	8	4.441	4.462	0.069	0.00	S
sn98dv	272.283	-40.300	0.1550	Anon	8	4.667	4.706	0.124	0.42	S
sn98dw	143.355	-77.658	0.0490	A0151	8	4.167	4.208	0.051	0.00	S
sn98dx	77.674	26.667	0.0538	U11149	11	4.208	4.175	0.030	0.05	JT
sn98dz	247.207	-56.375	0.0910	Anon	8	4.436	4.458	0.045	0.16	S
sn98ea	272.198	-39.821	0.0570	A3266	8	4.233	4.314	0.043	0.58	S
sn98ec	166.295	20.711	0.0200	U03576	11	3.778	3.801	0.039	0.57	JST
sn98ef	125.882	-30.566	0.0170	U00646	11	3.707	3.650	0.028	0.08	JST
sn98eg	76.464	-42.060	0.0234	U12133	11	3.846	3.897	0.042	0.26	JT
sn98es	143.189	-55.177	0.0095	N0632	11:20	3.455	3.438	0.031	0.33	JST
sn98fb	264.638	-51.045	0.0600	A3128	8	4.255	4.262	0.059	0.00	S
sn99Q	215.915	17.925	0.4600	Anon	31:3	5.140	5.336	0.042	0.07	RST
sn99U	238.552	30.694	0.5000	Anon	3	5.176	5.321	0.070	0.02	ST
sn99X	186.585	39.591	0.0257	C180022	11	3.887	3.888	0.037	0.33	JT
sn99aa	202.725	30.313	0.0157	N2595	11:20:15	3.673	3.684	0.032	0.01	RST
sn99ac	19.883	39.943	0.0099	N6063	11:20	3.472	3.478	0.023	0.42	JST
sn99ao	243.830	-20.023	0.0550	A3392	8	4.217	4.242	0.039	0.26	S
sn99by	166.914	44.120	0.0027	N2841	6:20	2.908	3.067	0.167	0.72	ST
sn99cc	59.667	48.740	0.0316	N6038	11	3.977	3.983	0.029	0.13	RJST
sn99cl	282.270	76.509	0.0082	N4501	15	3.391	3.009	0.090	1.68	RS
sn99cp	334.851	52.708	0.0104	N5468	15	3.494	3.525	0.026	0.04	RJT
sn99cw	101.768	-67.906	0.0112	M-010201	11	3.526	3.469	0.034	0.17	J
sn99da	89.732	32.649	0.0121	N6411	14:20	3.560	3.623	0.044	0.58	RJST
sn99dk	137.349	-47.464	0.0141	U01087	14	3.626	3.686	0.039	0.07	RT
sn99dq	152.839	-35.871	0.0136	N0976	11:20	3.610	3.548	0.023	0.35	JST
sn99ef	125.719	-50.086	0.0380	U00607	11	4.057	4.147	0.033	0.03	JT
sn99ej	130.442	-28.946	0.0127	N0495	11	3.581	3.684	0.031	0.08	JT
sn99ek	189.403	-8.234	0.0176	U03329	11	3.722	3.687	0.044	0.62	JT
sn99ff	168.784	-52.949	0.4550	Anon	35	5.135	5.289	0.048	0.16	RST
sn99fh	166.731	-53.793	0.3690	Anon	35	5.044	5.135	0.061	0.70	ST
sn99fj	166.879	-53.734	0.8150	Anon	35	5.388	5.564	0.051	0.09	RST
sn99fk	166.405	-53.167	1.0560	Anon	35	5.500	5.659	0.054	0.03	RST
sn99fm	167.075	-52.994	0.9490	Anon	35	5.454	5.580	0.053	0.04	RST
sn99fn	188.216	-31.901	0.4770	Anon	35	5.155	5.249	0.039	0.17	RST

4. Cosmological Implications

4.1. Hubble Diagrams

At a redshift of 0.5, the difference in luminosity distance between a flat and open universe with $\Omega_M = 0.3$ is 0.22 mag. With 230 SN Ia and 79 at redshifts greater than 0.3, we might expect to be able to distinguish between these cosmologies at better than 6σ . The real concern, however, is whether we are making a systematic error or hitting a systematic noise floor for SN Ia, and that we are fooling ourselves in thinking that we are making progress by averaging together more and more SN Ia.

The goal of this particular campaign was to strive to find and follow SN Ia at distinctly higher redshift than the majority of results at $z = 0.5$, since the effect of a dark-energy dominated cosmology looks very different from most plausible systematic effects at $z \approx 1$. If the universe really has no dark energy and the dimness of SN Ia by 0.22 mag at $z = 0.5$ is the result of a systematic error proportional to the redshift, one might expect SN Ia to be dimmer by 0.44 mag at $z = 1$ instead of 0.26 mag which would be the case for a flat universe.

Figure 8 shows the results from this campaign plotted over the full set of data from Table 15. Evidently there is a tendency for the SN Ia to be brighter at $z > 0.9$ (although the uncertainties are still large), suggesting that we are truly seeing a change in the deceleration of the universe and the effects of dark energy.

Given the heterogeneous nature of the data and the continual worry about non-Gaussian distributions, it is difficult to be quantitative about how well we can reject the possibility that we are seeing a systematic error in SN Ia brightness in a universe with no dark energy, and we discuss this in more detail below.

The scatter of the points from Table 15 obscures the trend with redshift, so we take medians over redshift bins and illustrate the result in Figure 9. Our redshift bins are derived from the data by choosing bins which have at least 12 SN Ia and a bin width of more than 0.25 in $\log z$ but no more than 50 SN Ia. The uncertainties, estimated from the 68% percentiles of the scatter of the points in each bin, are all less than 0.05 mag except for 0.08

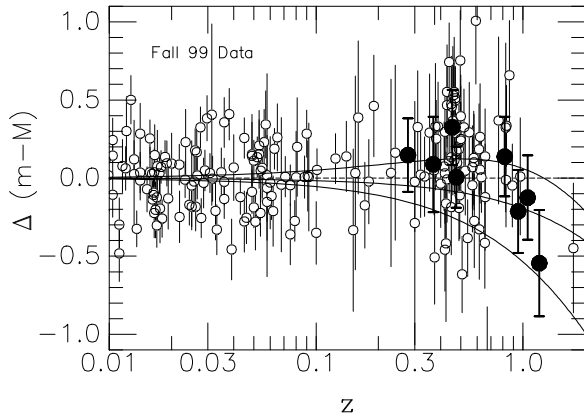


Fig. 8.— The Fall 1999 and other data points are shown in a residual Hubble diagram with respect to an empty universe. From top to bottom the curves show $(\Omega_M, \Omega_\Lambda) = (0.3, 0.7)$, $(0.3, 0.0)$, and $(1.0, 0.0)$, respectively, and the Fall 1999 points are highlighted.

mag in the highest z bin. We believe that this is approximately where systematics will start to dominate statistical error. That the points mostly lie below the $(0.3, 0.7)$ cosmology gets at the heart of what we believe may be the systematic uncertainty floor of the SN Ia distances in Table 15; we discuss this below. Nevertheless, we are apparently starting to see SN Ia become brighter at $z \approx 0.9$, rather than becoming ever dimmer because of a systematic effect.

4.2. Cosmological Parameters

We can fit the data from Table 15 with a variety of cosmological models. We do not want to fit all 230 SN Ia because the nearby ones are affected by peculiar motions which are beyond the scope of this paper to characterize. However, we do need to allow for the velocity uncertainty in modeling, so when we compute χ^2 we add 500 km s^{-1} divided by the redshift in quadrature to the distance error. For all fits we report χ^2 at the minimum as a function of H_0 , since this is equivalent to marginalizing over H_0 .

Fitting all 230 SN Ia yields $\chi^2 = 252$. If we restrict our fits to $z > 0.01$, we obtain $\chi^2 = 206$ for 195 points. We are also very wary of “extinguished” SN Ia since we are not certain we understand host extinction and reddening very well,

TABLE 15—*Continued*

SN	l^{II}	b^{II}	z	Host	Ref. ^a	$\log(cz)$	$\langle \log(dH_0) \rangle$	\pm	$\langle A_V \rangle$	Contrib
sn99fv	84.298	-56.405	1.1990	Anon	35	5.556	5.651	0.068	0.24	RST
sn99fw	84.665	-56.682	0.2780	Anon	35	4.921	5.007	0.047	0.34	RST
sn99gd	198.835	33.977	0.0190	N2623	11	3.756	3.779	0.029	1.27	JT
sn99gh	255.048	23.736	0.0088	N2986	11	3.421	3.356	0.023	0.15	JST
sn99gp	143.251	-19.504	0.0260	U01993	11:20:14	3.892	3.933	0.028	0.15	RJST
sn00B	166.353	22.791	0.0193	N2320	11	3.762	3.740	0.039	0.38	JST
sn00bk	295.292	55.233	0.0266	N4520	14	3.902	3.911	0.030	0.26	RJT
sn00ce	149.096	32.004	0.0165	U04195	11:14	3.694	3.705	0.030	1.02	RJT
sn00cf	99.883	42.165	0.0360	M+111925	11	4.033	4.112	0.032	0.13	RJST
sn00cn	53.445	23.318	0.0233	U11064	11	3.844	3.847	0.023	0.27	JST
sn00cx	136.506	-52.482	0.0070	N0524	11:19	3.322	3.320	0.023	0.02	RST
sn00dk	126.834	-30.344	0.0164	N0382	11	3.692	3.677	0.023	0.01	JST
sn00dz	84.367	-56.390	0.5000	Anon	13	5.176	5.352	0.053	0.07	RST
sn00ea	167.211	-61.402	0.4200	Anon	13	5.100	5.091	0.053	0.88	RST
sn00ec	166.295	-60.176	0.4700	Anon	13	5.149	5.340	0.043	0.04	RST
sn00ee	166.045	-53.429	0.4700	Anon	13	5.149	5.343	0.041	0.04	RST
sn00eg	167.097	-53.108	0.5400	Anon	13	5.209	5.236	0.049	0.17	RST
sn00eh	188.297	-31.651	0.4900	Anon	13	5.167	5.224	0.042	0.20	RST
sn00fa	194.167	15.479	0.0218	U03770	11	3.815	3.837	0.026	0.34	JST
sn01V	218.929	77.733	0.0162	N3987	22	3.686	3.662	0.023	0.20	JST

^a References: (1) Boffi et al. 2003 (in preparation); (2) Buta & Turner 1983, PASP, 95, 72, and Tsvetkov 1982, SvAL, 8, 115; (3) Clocchiatti et al. 2003 (in preparation); (4) Filippenko et al. 1992, AJ, 104, 1543, and Leibundgut et al. 1993, AJ, 105, 301, and Turatto et al. 1996, MNRAS, 283, 1; (5) Ford et al. 1993, AJ, 106, 3; (6) Garnavich et al. 2001, astro-ph/0105490; (7) Germany 2001 (PhD thesis ANU); (8) Germany et al. 2003, A&A, in press; (9) Hamuy et al. 1991, AJ, 102, 208; (10) Hamuy et al. 1996, AJ, 112, 2408; (11) Jha 2002 (PhD thesis Harvard); (12) Jha et al. 1999, ApJS, 125, 73, and Suntzeff et al. 1999, AJ, 117, 1175; (13) Jha et al. 2003, ApJ (in preparation); (14) Krisciunas 2001, AJ, 122, 1616; (15) Krisciunas et al. 2000, ApJ, 539, 658; (16) Leibundgut et al. 1991, A&AS, 89, 537; (17) Leibundgut et al. 2003 (in preparation); (18) Li et al. 1999, AJ, 117, 2709; (19) Li et al. 2001, PASP, 113, 1178; (20) Li et al. 2004, (in preparation); (21) Lira et al. 1998, AJ, 115, 234; (22) Mandel et al. 2001, AAS, 199, 4704; (23) Modjaz et al. 2001, PASP, 113, 308; (24) Norgaard-Nielsen et al. 1989, Nature, 339, 523; (25) Perlmutter et al. 1999, ApJ, 517, 565; (26) Phillips et al. 1997, PASP, 99, 592; (27) Richmond et al. 1995, AJ, 109, 2121, and Patat et al. 1996, MNRAS, 278, 111, and Meikle et al. 1996, 281, 263; (28) Riess et al. 1998 AJ, 116, 1009; (29) Riess et al. 1998, ApJ, 504, 935; (30) Riess et al. 1999, AJ, 117, 707; (31) Riess et al. 2000, ApJ, 536, 62; (32) Riess et al. 2001, ApJ, 560, 49; (33) Suntzeff 2001 (private communication); (34) Suntzeff et al. 2003 (in preparation); (35) Tonry et al. 2003, ApJ (this paper); (36) Turatto et al. 1998, AJ, 116, 2431; (37) Wells et al. 1994, AJ, 108, 2233

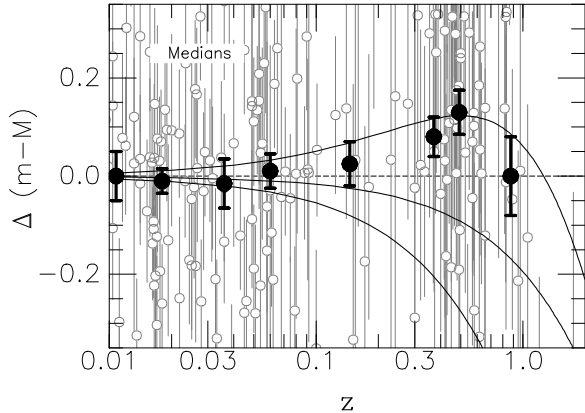


Fig. 9.— The Fall 1999 and other data points are shown in a residual Hubble diagram with respect to an empty universe. In this plot the highlighted points correspond to median values in eight redshift bins. From top to bottom the curves show $(\Omega_M, \Omega_\Lambda) = (0.3, 0.7)$, $(0.3, 0.0)$, and $(1.0, 0.0)$, respectively.

¹⁹ and we are mindful of the covariance between A_V and d . If we further restrict the sample to $A_V < 0.5$ mag we get $\chi^2 = 169.5$ for 172 SN Ia, and we regard this as the most useful sample for deriving cosmological parameters. There are further cuts which could be made: exclusion of the SCP data points (where there is no information on host galaxy extinction) gives us $\chi^2 = 121.6$ for 130 SN Ia. However the constraints on cosmological parameters do not change significantly and we are concerned about acquiring systematic problems along with spurious precision.

¹⁹Phillips et al. (1999) give in their Table 2 the Galactic and host reddening $E(B - V)$ for nearby supernovae. If, as suggested by the 44 SN Ia studied by Jha (2002, §3), most SN Ia obey Lira’s (1995) relation, then the colors at maximum and in the tail of the $B - V$ color curve *can* give us a good handle on the *reddening* at optical wavelengths. However, while most galaxies may have dust like that in our Galaxy, with $R_V \equiv A_V/E(B - V) \approx 3.1$ (Cardelli et al. 1989), there are heavily reddened objects such as SN 1999cl whose host galaxy has dust with $R_V < 2$ (Krisciunas et al. 2001). Furthermore, high-redshift supernovae are typically too faint to detect with sufficient precision 30 to 90 rest-frame days after maximum light. Finally, while a combination of optical and infrared data gives us a good handle on the extinction A_V (Krisciunas et al. 2000, 2001, 2003), SN Ia with $z \gtrsim 0.10$ are too faint in the rest-frame H -band and K -band even for 10-m class telescopes to apply the V minus infrared method of determining extinction.

In the analyses that follow we use various subsamples of the 172 SN Ia with $z > 0.01$ and $A_V < 0.5$ mag. For each calculation we determine χ^2 as a function of H_0 , Ω_M , and Ω_Λ . Given that χ^2/N is close to unity, we convert this to a probability as $\exp(-0.5\chi^2)$, normalize, marginalize over H_0 , and locate contours of constant probability density which enclose 68%, 95%, and 99.5% of the probability. In those calculations where we additionally constrain cosmology by using the galaxy clustering shape measurements, we use observations from the 2dF redshift survey (Percival et al. 2001), $\Omega_M h = 0.20 \pm 0.03$, and $H_0 = 72 \pm 8$ km s⁻¹ Mpc⁻¹ (Freedman et al. 2001). In all cases, contours are calculated for a cosmological constant equation of state ($w = -1$).

Figure 10 shows these contours for a sample of 94 SN Ia ($\chi^2 = 103$) which include only the recent results from Leibundgut et al. (2003), Suntzeff et al. (2003), Jha et al. (2003b), and the data presented here. The error ellipses are virtually identical to those drawn by Riess et al. (1998) and Perlmutter et al. (1999), although the data and analyses are completely different, confirming the conclusion that the universe is accelerating. This independent sample gives a consistent result: the acceleration inferred several years ago was not a statistical fluke.

Figure 11 shows these contours for the sample of 130 SN Ia ($\chi^2 = 122$) which includes all the SN Ia which have been published by the HZT.

Figure 12 shows these contours for the sample of 172 SN Ia ($\chi^2 = 170$) which includes all the SN Ia for which we have either data or published results.

In all cases, the derived probability contours with a 2dF prior are remarkably tightly constrained to the $\Omega_{tot} = 1$ line which is being delineated so well by CMB observations.

As with previous results from SN Ia, the approximate combination $\Omega_\Lambda - \Omega_M$ is relatively well constrained. For these data

$$\Omega_\Lambda - 1.4\Omega_M = 0.35 \pm 0.14.$$

However, the presence of these higher-redshift observations from Fall 1999 as well as SN 1997ff (Riess et al. 2001) has started to close off the contours from running away to very large Ω . If we assume a flat universe as well as $w = -1$, the

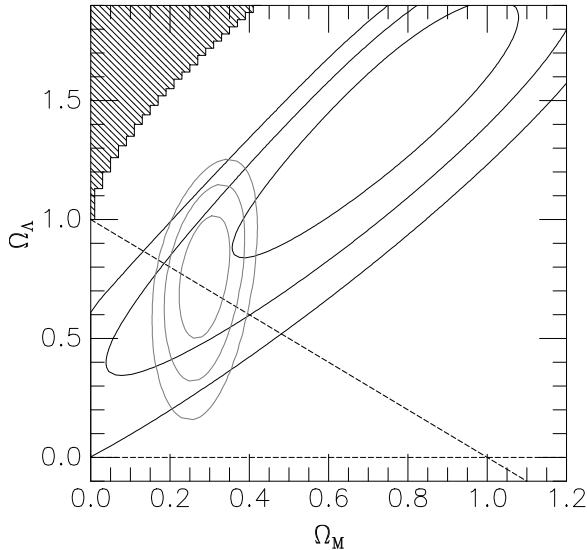


Fig. 10.— Probability contours for Ω_Λ versus Ω_M are shown at 1σ , 2σ , and 3σ with $w = -1$. We also give 1σ , 2σ , and 3σ contours when we adopt a prior of $\Omega_M h = 0.20 \pm 0.03$ from the 2dF survey (Percival et al. 2001). These constraints use only the 26 new SN Ia at $z > 0.3$ (which are completely independent of any which have been used before for cosmological constraints).

SN Ia data require $\Omega_M = 0.28 \pm 0.05$, independent of large-scale structure estimates.

We can also fit for the equation of state of the dark energy, $p = w\rho$, where $w = 1/3$ for radiation, $w = 0$ for pressureless matter (e.g., cold dark matter), $w = -1$ for a cosmological constant, etc. Restricting ourselves to $\Omega_{tot} = 1$, Figure 13 shows the contours for Ω_M and w , with and without the 2dF prior.

Dark energy candidates with $w > -2/3$ are strongly disfavored by these data. Figure 14 shows the data from Figure 13 marginalized over Ω_M . The combination of SN Ia and constraints on Ω_M from large scale structure puts a sharp constraint on how positive w can be. The 95% confidence limits on w lie in the range $-1.48 < w < -0.72$. If we additionally adopt a prior that $w > -1$, we find that $w < -0.73$ at 95% confidence. These constraints are again very similar to recent results reported using the WMAP satellite: $w < -0.78$ at 95% confidence for priors of $w > -1$ and Ω_M from the 2dF redshift survey (Spergel et al. 2003).

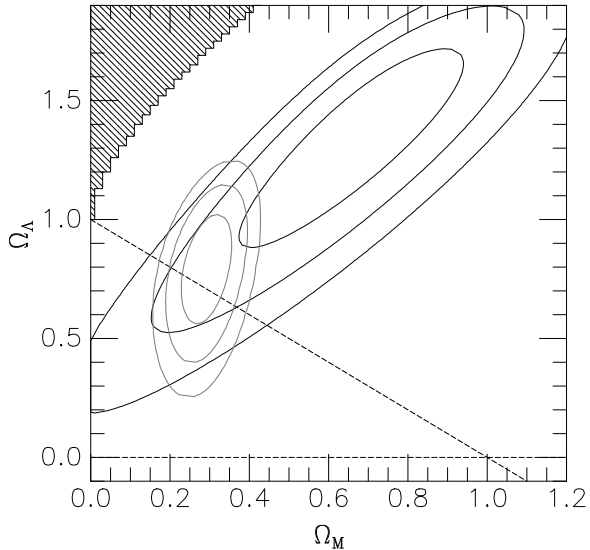


Fig. 11.— Probability contours for Ω_Λ versus Ω_M are shown at 1σ , 2σ , and 3σ with $w = -1$. We also give 1σ , 2σ , and 3σ contours when we adopt a prior of $\Omega_M h = 0.20 \pm 0.03$ from the 2dF survey (Percival et al. 2001). These constraints use the 113 SN Ia published by the HZT.

Since the gradient of $H_0 t_0$ is nearly perpendicular to the narrow dimension of the Ω_Λ - Ω_M contours, we obtain a surprisingly good estimate of $H_0 t_0$, illustrated in Figure 15. We find that $H_0 t_0 = 0.96 \pm 0.04$. Although independent measurements of these parameters do not approach this precision yet, for comparison we note that $h = 0.72 \pm 0.08$ from Freedman et al. (2001) corresponds to a Hubble time of $H_0^{-1} = 13.6 \pm 1.5$ Gyr. Krauss & Chaboyer (2002) have recently found a median age of 12.5 Gyr for 17 metal-poor globular clusters. If these globular clusters formed 0.6 Gyr after the Big Bang, then the universe has $t_0 = 13.1$ Gyr, consistent with a world model with $h = 0.72$, $\Omega_M = 0.3$, and $\Omega_\Lambda = 0.7$. The assumed globular cluster incubation time of 0.6 Gyr corresponds to an epoch of star formation we would observe now at $z \approx 8$. Adopting an uncertainty of ± 2 Gyr for t_0 , the product $H_0 t_0 = 0.96 \pm 0.19$. We also note that remarkable agreement with the WMAP result for the age of the universe: 13.7 ± 0.2 Gyr (Spergel et al. 2003).

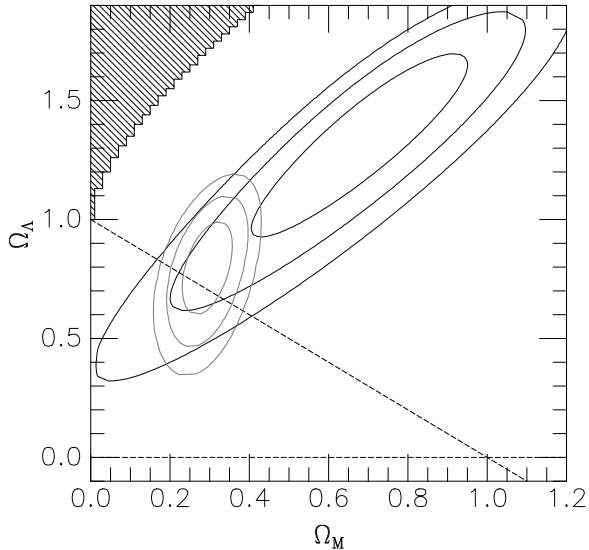


Fig. 12.— Probability contours for Ω_Λ versus Ω_M are shown at 1σ , 2σ , and 3σ with $w = -1$. We also give 1σ , 2σ , and 3σ contours when we adopt a prior of $\Omega_M h = 0.20 \pm 0.03$ from the 2dF survey (Percival et al. 2001). These constraints use the full sample of 172 SN Ia with $z > 0.01$ and $A_V < 0.5$ mag.

5. Discussion

5.1. Testing systematics

Drell, Loredó, & Wasserman (2000) (DLW) wrote a very thoughtful critique of the then extant SN Ia data, questioning whether a cosmological constant was required or a systematic error could account for the observations. We present here more than twice as many objects with improved error estimates. We believe that some of the points noted by DLW are simply caused by selection effects, for example the observed diminution of the range of Δ with redshift. However, their point that a large systematic shift in the luminosity of supernovae with redshift, coupled with a large positive Ω_M could fit the data nearly as well as a universe with a cosmological constant, is still valid.”

Using our preferred sample of 172 SN Ia we reevaluate the Bayesian odds factor between a model “FRW” with no systematic error and a cosmological constant and a “Model II” with no cosmological constant but a systematic error which

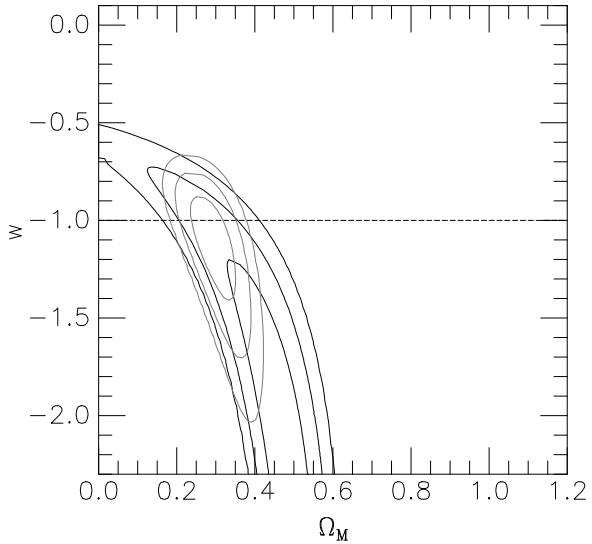


Fig. 13.— Probability contours for dark energy parameter w versus Ω_m are shown at 1σ , 2σ , and 3σ when $\Omega_{tot} = 1$. We also give 1σ , 2σ , and 3σ contours when we adopt a prior of $\Omega_M h = 0.20 \pm 0.03$ from the 2dF survey (Percival et al. 2001). This sample includes all 172 SN Ia with $z > 0.01$ and $A_V < 0.5$ mag.

goes as a power law of $(1+z)$ (i.e., the distance modulus has a systematic error term of $\beta \ln(1+z)$ — this is the DLW “Model II”). When we integrate both models over H_0 , Ω_M , and either Ω_Λ or β and divide by plausible prior ranges for these parameters, we get an odds factor of 29 in favor of the FRW model. Most would interpret this as “pretty good” odds that the FRW model is to be preferred over a systematic error, but not extremely strong odds.

However, in this Bayesian framework, the ratio of the probabilities for the two models also includes the ratio of the prior probabilities. The systematic model can match the observations reasonably well, but it does so only for $\Omega_M \approx 1$ and a β which corresponds to a systematic which rises to 0.7 mag at $z = 1$. Both of these parameters seem out of step with other lines of investigation and would be quite disfavored by reasonable priors.

We certainly do not expect that Ω_M could be anywhere near unity. The evidence against this comes from the observations that the $H_0 t_0$ product appears to be much larger than $2/3$, and there is ample evidence on many scales that there is

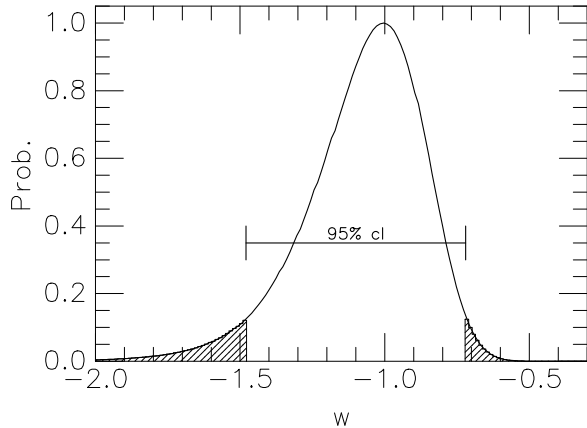


Fig. 14.— The probability distribution for w using the 2dF prior, marginalized over Ω_M . The 95% confidence limits are $-1.48 < w < -0.72$.

nowhere near as much mass as $\Omega_M = 1$ in clustered form (e.g., Blakeslee et al. 1999; Percival et al. 2001).

The argument against such a very large systematic error (0.7 mag at $z = 1$) is theoretical and empirical. We work with SN Ia precisely because they are dead stars which should have very little difference between today and 7 Gyr ago, and we certainly do not have any theoretical expectation that explosions have become a factor of 2 dimmer in the mean over the previous 7 Gyr.

Empirically, we argue that the SN Ia we see locally should have at least the range of properties seen at $z = 1$ because there are low metallicity systems today and there appear to be SN Ia which are exploding quite promptly (e.g., NGC 5253 at $0.1 L^*$ had a starburst recently and has had 2 SN Ia in the past century). Likewise, if SN Ia were as much as a factor of 2 dimmer in the past, we would expect there to be a significant dispersion — surely *some* of the SN Ia at $z = 1$ would produce explosions comparable to those of today.

We are always cognizant of the possibility of observational systematic error or problems with our analysis, but 0.7 mag is considerably beyond what we think might be possible.

The exact factor by which Model II would therefore be disfavored according to these prior considerations is subjective since the place where the systematic probability is becoming sizable is out on the tails of the priors we assign for Ω_M and

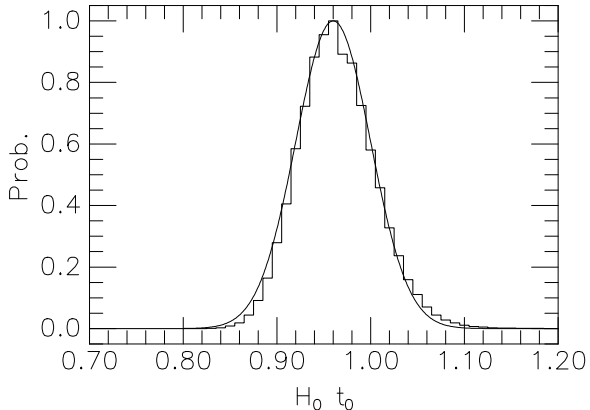


Fig. 15.— The probability distribution for $H_0 t_0$ given the SN Ia observations is tightly constrained to 0.96 ± 0.04 , and an approximating Gaussian curve.

β . We think it is not worthwhile to try to assign a quantitative probability to these, other than to note that the factor by which the net probability of Model II relative to Model FRW will be disfavored will be significantly higher than the factor of 29 from the integrated likelihoods.

Therefore we believe that we have very strong evidence that a systematic effect which goes as a power law of $(1+z)$ is not likely to match the SN Ia data. In particular, a simple gray or intergalactic dust model does not appear to be viable, and evolutionary effects such as metallicity, C/O ratio, or host dust properties which change smoothly and monotonically with z are also likely not to fit the data as well as an FRW cosmology.

It is always possible to imagine a systematic error which is tuned to match the FRW turnover near $z = 1$, but it might be less a priori plausible than a simple $(1+z)$ power. However, a proper Bayesian analysis would have to take into account the volume of the space from which such a model was drawn and the model might be disfavored for that reason, even though it might fit the SN Ia data very well.

5.2. Selection and Other Effects

The Fall 1999 survey went deeper and redder than any previous campaign. As a result we did start to see extinguished SN Ia at $z \approx 0.5$ and we expect that we are less subject to selection bias.

Our model for rates seems to work remarkably well, suggesting that there is not a rare population of luminous objects which we do not know about from local samples. The exceptions are SN 1999fo (Gertie) and SN 1999fu (Alvin), which were not SN Ia, but were definitely unusual, flux-variable objects.

At face value the average absorption of the distant supernovae is significantly smaller than for the nearby sample. Out to $z \leq 0.3$ the 151 supernovae suffered an average absorption of $\langle A_V \rangle = 0.35 \pm 0.50$ mag, while the 37 distant supernovae with $z > 0.3$ average $\langle A_V \rangle = 0.20 \pm 0.23$ mag. There is a large scatter in these averages, but the offset is 0.15 mag. The distribution of absorption values for the nearby supernova sample has a long tail to higher absorptions, which is missing for the distant sample. However, the distribution of absorptions of the distant supernovae is much narrower. Most probably this is a signature of the magnitude-limited searches, where heavily obscured supernovae are not detected. Selecting the 130 objects (172 less 42 SCP SN Ia without host extinctions) which were used to construct the likelihood functions ($z > 0.01$ and $A_V < 0.5$ mag), we find that the averages decrease to $\langle A_V \rangle = 0.17 \pm 0.14$ mag for the nearby supernovae and $\langle A_V \rangle = 0.14 \pm 0.11$ mag for the distant ones. The difference has decreased to less than 0.03 mag and clearly the faintness of the distant supernovae cannot be attributed to errors in the treatment of absorption. In fact, more absorption would make the distant supernovae more luminous and move them to larger distances. The small average absorption argues that the distant objects indeed are at larger distances than for an empty universe model, in agreement with the results from Riess et al. (2000), Leibundgut (2001), and Sullivan et al. (2003).

Of the objects at $z > 0.8$ in our large data set, several objects (principally those discovered before 1999) rely on rest-frame U -band data to measure extinction. The rest-frame U -band data have a number of uncertainties, including less certain K -corrections, greater susceptibility to extinction, and less well studied behavior. Most importantly, the SN Ia have less intrinsic uniformity in the U bandpass. For the data set presented here, the average measured distance to those objects using the U band as a primary source of information for

distance measurement is further than to those objects which do not rely on U -band data, but the difference is not statistically significant. These effects will be further discussed in Jha et al. (2003c) and Suntzeff et al. (2003).

We have not corrected these data for gravitational lensing. It should be negligible at these redshifts, but will become much more serious as we push to higher redshift.

Nevertheless, we do think we can start to perceive systematic errors in the data at the 0.04 mag level. The contours seen in Figures 10–12 have their most probable Ω_M, Ω_Λ well offset from the Ω_M indicated by the 2dF survey and a flat universe. This is not a failure of our probability analysis. We have performed extensive Monte Carlo tests on simulated data sets and we recover Ω_M, Ω_Λ with very little bias. What drives our best fit solution to high values of Ω_M, Ω_Λ is the fact that the data make a very fast transition from recent acceleration to earlier deceleration, i.e. the transition from the faintness at $z \sim 0.5$ to the brightness at $z \sim 1$ is very fast. The contours in Figures 10–12 are quite shallow in the $\Omega_M + \Omega_\Lambda$ direction, and a systematic error of 0.04 mag is quite sufficient to move our most probable values for Ω_M, Ω_Λ to these high values. This may be a statistical fluke at the 1.5- σ level, although the systematic offsets of the points in Figure 9 from a cosmological line may point to systematic errors.

We have described some of the possible culprits for such a systematic above. Selection biases because of UV selection or any of the other practical difficulties in carrying out a supernova search are always a worry, particularly since they are so hard to quantify and because SN Ia are so non-uniform in the UV. Photometric and K -correction errors are certainly possible, since absolute photometry of objects with non-stellar SEDs at $m > 20$ is *extremely* hard to achieve at the 0.01 mag level. It is conceivable that gravitational lensing is more important than has been estimated; we expect that the SN Ia found by the GOODS survey will offer a strong test of this. Most likely there is a variety of errors throughout this very heterogeneous set of data, and the best way forward is acquisition of new data from well designed observations which are taken and analyzed with more care. Although the basic conclusion that the Universe is accelerating is not in jeopardy since the $\Omega_M - \Omega_\Lambda$

direction is relatively insensitive to systematic error, we remain wary of over interpretation of the extant SN Ia data and urge others to do the same.

5.3. Comparison with the CMB

As this paper was nearing completion, the WMAP team reported new results from a high angular resolution all-sky map of structure (Spergel et al. 2003). Their main conclusions, namely that we live in a geometrically flat Universe with Ω_{total} , Ω_M , and Ω_Λ of 1.00, 0.73, and 0.27, respectively, are entirely consistent with the results presented here. This convergence of results lends great strength to what is emerging as the new “Standard Model” of contemporary cosmology, in which the role of matter is secondary to the accelerating expansion driven by dark energy.

Ascertaining the physical mechanism that is responsible for this accelerating expansion is one of the crucial next steps for observational cosmology. Since supernovae are well suited to probing precisely the redshift range over which Λ begins to dominate, new projects are being undertaken to exploit this.

5.4. What Next? The Future

Future campaigns to observe SN Ia at high redshift will focus on three themes: refining measures of luminosity distance, understanding and controlling systematic errors, and learning about SN Ia physics. The payoff for measuring luminosity distances accurately is that we can determine the equation of state of the dark energy and whether it has changed as a function of time (redshift). There is certainly a systematic floor to our ability to determine distances from SN Ia, but we do not yet know what it is. It appears that gray dust is not an issue, but gravitational lensing, for example, is certainly a contaminant.

Opinions differ as to where the incompletely understood SN Ia physics causes a cosmic scatter which does not average out, but most would agree it lies in the range of 0.02–0.04 mag. This implies that the luminosity distance at a given redshift is not improved by observing more than 25–100 SN Ia at that redshift. There are many outstanding questions about SN Ia physics which may best be approached by observations of SN Ia at high redshift. Measuring SN Ia rates and com-

parison with the star-formation rate may elucidate the SN Ia explosion mechanism, SN Ia progenitors, and gestation period. The distribution of SN Ia parameters as a function of redshift may also be useful for understanding SN Ia and host galaxy physics.

The HZT, in collaboration with the Surf’s-Up group at the IfA, undertook a six-month survey of 2.5 deg² in R , I , and Z . Many SN Ia as well as other transient objects were discovered and followed (Barris et al. 2003). Members of the HZT have begun the ESSENCE survey (Smith et al. 2002) to discover and follow 200 SN Ia in the range $0.1 < z < 0.8$ with the goal of measuring the equation of state parameter w of the dark energy to $\pm 10\%$. Riess et al. (2003) have an ongoing program with *HST* and the GOODS survey, using the Advanced Camera for Surveys (ACS) to discover and follow approximately 6 SN Ia at $z \approx 1.4$. This will be exceedingly powerful for measuring the effects of dark energy, understanding systematics, and constraining any time evolution of w . The CFHT Legacy Survey (<http://www.cfht.hawaii.edu/Science/CFHLS/>) has the goal of finding and following ~ 2000 SN Ia in multiple colors. The Lick Observatory Supernova Search (LOSS; Filippenko et al. 2001) is finding and monitoring record numbers of very nearby supernovae, with 82 in 2002 alone (<http://astro.berkeley.edu/~bait/kait.html>). The Nearby Supernova Factory (Aldering et al. 2002) will obtain spectrophotometry for ~ 300 nearby SN Ia, suitable for K-corrections of high-redshift supernovae and for exploring SN Ia physics and systematics. In the near future, Pan-STARRS (Kaiser et al. 2002) should discover and follow a vast number of SN Ia ($> 10^4$ per year). Finally, in the more distant future, the proposed SNAP satellite (Nugent 2001) would follow several thousand objects with an experiment designed to minimize observational systematic errors, limited only by the floor imposed by nature. The future indeed looks bright for cosmological and related studies of SN Ia.

We thank the staffs at many observatories for their assistance with the observations. Financial support for this work was provided by NASA through programs GO-08177, GO-08641, and GO-09118 from the Space Telescope Science Insti-

tute, which is operated by the Association of Universities for Research in Astronomy, Inc., under NASA contract NAS 5-26555. Funding was also provided by National Science Foundation grants AST-9987438 and AST-0206329. A.C. acknowledges the support of CONICYT (Chile) through FONDECYT grant Nos. 1000524 and 7000524. This paper uses data from the Sloan Digital Sky Survey (SDSS) early data release.

6. Appendix A

6.1. $N(N-1)/2$ differences

We use the Alard & Lupton (1998) code to convolve one image to match the other. We fit a suitable star in one of these images with the Schechter “Waussian” (inverse of a truncated Taylor series for e^{x^2}) to derive a standard PSF. Since we know where the supernova is located, we do a two-parameter fit (peak and sky) of this standard PSF, and we scale the flux measured in the standard star by the ratio of the fit peaks to derive a supernova flux difference for these two images. We also select roughly ten other locations in the image and insert a copy of the standard star scaled to match the supernova flux, and pick it up again using the same procedure of two-parameter fits. This tells us of any bias (we do not see any) and gives us an estimate of the flux error for this pair of images.

Applying this procedure to all $N(N-1)/2$ pairs creates an $N \times N$ antisymmetric matrix of flux differences, and a symmetric matrix of errors. We also choose approximately a dozen stars for each supernova field which are bright enough to have good S/N in all images but faint enough not to be saturated, and perform a PSF flux measurement for all stars in all images. Matching up these tables of stars, we can form a mean flux scale between all pairs of images, and then assemble another $N \times N$ antisymmetric matrix of magnitude differences. The flux differences are all put on a common scale using the magnitude differences.

Finally, we fit these antisymmetric matrices as the difference between the i^{th} and j^{th} entries of an N vector. We derive two sets of error estimates: the first is based on the pairwise flux error estimates and the second comes from the residuals between the observed difference matrix and the matrix assembled by differencing the terms of

the resultant vector. These estimates are generally consistent with one another, although the observed errors reflect the uncertainties of the individual observations and the mismatch errors give a broader view of the inconsistency of any observation with the others.

REFERENCES

- Aguirre, A. 1999a, ApJ, 512, 19
- Aguirre, A. 1999b, ApJ, 525, 583
- Alard, C., & Lupton, R. H. 1998, ApJ, 503, 325
- Aldering, G., et al. Proceeding of the SPIE conference on Astronomical Instrumentation, Kona, August 2002
- Barris, B., et al. 2002, BAAS, 34, 4, 1306
- Benítez, N., Riess, A., Nugent, P., Dickinson, M., Chornock, R., & Filippenko, A. V. 2002, ApJ, 577, 1
- Blakeslee, J. P., Davis, M., Tonry, J. L., Dressler, A., & Ajhar, E. A. ApJ, 527, 73
- Boffi, F., et al. 2003, in preparation
- Burstein, D., & Heiles, C. 1984, ApJS, 54, 33
- Buta, R. J., & Turner, A. 1983, PASP, 95, 72
- Candia, P., et al. 2003, PASP, in press
- Cappellaro, E., Evans, R., & Turatto, M. 1999, A&A, 351, 459
- Cardelli, J. A., Clayton, G. C., & Mathis, J. S. 1989, ApJ, 345, 245
- Carroll, S. M. 2001 <http://www.livingreviews.org/Articles/Volume4/2001-1carroll>
- Clocchiatti, A., et al. 2003, in preparation
- Coil, A. L., et al. 2000, ApJ, 544, 111
- Cousins, A. W. J. 1976, Mem. R. Astron. Soc., 81, 25
- de Bernardis, P., et al. 2002, ApJ, 564, 559
- Dolphin, A. E. 2000, PASP, 112 1397
- Drell, P. S., Lored, T. J., & Wasserman, I. 2000, ApJ, 530, 593

- Falco, E. E., et al. 1999, *ApJ*, 523, 617
- Filippenko, A. V. 1997, *ARAA*, 35, 209
- Filippenko, A. V., Li, W. D., Treffers, R. R., & Modjaz, M. 2001, in *Small-Telescope Astronomy on Global Scales*, ed. W. P. Chen, C. Lemme, & B. Pacynski (San Francisco: ASP), 121
- Filippenko, A. V., & Riess, A. G. 2001, in *Particle Physics and Cosmology: Second Tropical Workshop*, ed. J. F. Nieves (New York: AIP), 227
- Filippenko, A. V., et al. 1992, *AJ*, 104, 1543
- Filippenko, A. V., et al. 1995, *ApJ*, 450, L11
- Folkes, S., et al. 1999, *MNRAS*, 308, 459
- Ford, C. H., et al. 1993, *AJ*, 106, 1102
- Freedman, W., et al. 2001, *ApJ*, 553, 47
- Garnavich, P. M., et al. 1998a, *ApJ*, 493, 53
- Garnavich, P. M., et al. 1998b, *ApJ*, 509, 74
- Garnavich, P. M., et al. 2001, *astro-ph/0105490*
- Germany, L. M. 2001, Ph.D. Thesis, Australian National University
- Germany, L. M., et al. 2003, *A&A*, in press
- Goldhaber, G., et al. 2001, *ApJ*, 558, 359
- Gunn, J. E., & Stryker, L. L. 1983, *ApJS*, 52, 121
- Hamuy, M., Phillips, M. M., Maza, J., Suntzeff, N. B., Schommer, R. A., & Avilés, R. 1995, *AJ*, 109, 1
- Hamuy, M., Phillips, M. M., Suntzeff, N. B., Schommer, R. A., Maza, J., Smith, R. C., Lira, P., & Avilés, R. 1996b, *AJ*, 112, 2438
- Hamuy, M., et al. 1991, *AJ*, 102, 208
- Hamuy, M., et al. 1996a, *AJ*, 112, 2408
- Hatano, K., Branch, D., & Deaton, J. 1998, *ApJ*, 502, 177
- Höflich, P., Wheeler, J. C., & Thielemann, F.-K. 1998, *ApJ*, 495, 617
- Höflich, P., & Khokhlov, A. 1996, *ApJ*, 457, 500
- Holland, S. 1998, *AJ*, 115, 1916
- Jha, S. 2002, Ph.D. Thesis, Harvard University
- Jha, S., et al. 1999, *ApJS*, 125, 73
- Jha, S., et al. 2003a, in preparation
- Jha, S., et al. 2003b, in preparation
- Jha, S., Riess, A. G., & Kirshner, R. P. 2003c, in preparation
- Kaiser, N., et al. Proceeding of the SPIE conference on *Astronomical Instrumentation*, Kona, August 2002
- Kim, A., Goobar, A., & Perlmutter, S. 1996, *PASP*, 108, 190
- Kirshner, R. P., et al. 1993, *ApJ*, 415, 589
- Krauss, L. M., & Chaboyer, B. 2002, *Science*, in press (*astro-ph/0111597*) *Cosmology*, N. S. Netherington, ed. (New York and London: Garland), 218 (*errata astro-ph/9308025*)
- Krisciunas, K., Hastings, N. C., Loomis, K., McMillan, R., Rest, A., Riess, A. G., & Stubbs, C. 2000, *ApJ*, 539, 658
- Krisciunas, K., et al. 2001, *AJ*, 122, 1616
- Krisciunas, K., et al. 2003, *AJ*, 125, 166
- Kron, G. E., & Smith, J. L. 1951, *ApJ*, 113, 324
- Landolt, A. U. 1992, *AJ*, 104, 340
- Leibundgut, B. 1989, Ph.D. Thesis, Univ. of Basel
- Leibundgut, B., Tammann, G. A., Cadonau, R., & Cerrito, D. 1991, *A&AS*, 89, 537
- Leibundgut, B. 2001, *ARA&A*, 39, 67
- Leibundgut, B., et al. 2003, in preparation
- Leibundgut, B., et al. 1993, *AJ*, 105, 301
- Li, W. D., Filippenko, A. V., Treffers, R. R., Riess, A. G., Hu, J., & Qiu, Y. 2001a, *ApJ*, 546, 734
- Li, W. D., et al. 1999, *AJ*, 117, 2709
- Li, W. D., et al. 2001b, *PASP*, 113, 1178

- Li, W. D., et al. 2003, in preparation
- Lira, P. 1995, Master's thesis, Univ. of Chile
- Lira, P., et al. 1998, AJ, 115, 234
- Mandel, K., et al. 2001, BAAS, 199, 4704
- Marzke, R. O., da Costa, L. N., Pellegrini, P. S., Willmer, C. N. A., & Geller, M. J. 1998, ApJ, 503, 617
- Massey, P., Strobel, K., Barnes, J. V., & Anderson, E. 1988, ApJ, 328, 315
- Meikle, P., et al. 1996, 281, 263
- Modjaz, M., et al. 2001, PASP, 113, 308
- Nørgaard-Nielsen, H. U., Hansen, L., Jorgensen, H. E., Aragon Salamanca, A., & Ellis, R. S. 1989, Nature, 339, 523.
- Novicki, M. C., & Tonry, J. 2000, BAAS, 32, 1576
- Nugent, P. 2001, in Particle Physics and Cosmology: Second Tropical Workshop, ed. J. F. Nieves (New York: AIP), 263
- Nugent, P., Kim, A., & Perlmutter, S. 2002, PASP, 114, 803
- Oke, J. B., et al., 1995, PASP, 107, 375
- Paerels, F., Petric, A., Telis, G., & Helfand, D. J., 2002, BAAS, 34, 4, 1264
- Pain, R., et al. 1996, ApJ, 473, 356
- Pain, R., et al. 2002, ApJ, 577, 120
- Parodi, B. R., Saha, A., Sandage, A., & Tammann, G. A. 2000, ApJ, 540, 634
- Padmanabhan, T. 200, hep-th/0212290
- Patat, F., et al. 1996, MNRAS, 278, 111
- Peacock, J. A., et al. 2001, Nature, 410, 169
- Peebles, P. J. E., & Ratra, B. 2002, Rev. Mod. Phys., in press (astro-ph/0207347)
- Percival, W. J., et al. 2001, MNRAS, 327, 1297
- Perlmutter, S., et al. 1995, ApJ, 440, 41
- Perlmutter, S., et al. 1997, ApJ, 483, 565
- Perlmutter, S., et al. 1998, Nature, 391, 51
- Perlmutter, S., et al. 1999, ApJ, 517, 565
- Persson, S. E., Murphy, D. C., Krzeminski, W., Roth, M., & Rieke, M. J. 1998, AJ, 116, 2475
- Phillips, M. M. 1993, ApJ, 413, L105
- Phillips, M. M., Lira, P., Suntzeff, N. B., Schommer, R. A., Hamuy, M., & Maza, J. 1999, AJ, 118, 1766
- Pinto, P. A., & Eastman, R. G. 2000a, ApJ, 530, 744
- Pinto, P. A., & Eastman, R. G. 2000b, ApJ, 530, 757
- Rana, N. C. 1979, Ap&SS, 66, 173
- Rana, N. C. 1980, Ap&SS, 71, 123
- Richmond, M. W., et al. 1995, AJ, 109, 2121
- Riess, A. G., Press, W. H., & Kirshner, R. P. 1995, ApJ, 438, 17
- Riess, A. G., Press, W. H., & Kirshner, R. P. 1996, ApJ, 473, 88.
- Riess, A. G., et al. 1998a, AJ, 116, 1009
- Riess, A. G., Nugent, P., Filippenko, A. V., Kirshner, R. P., Perlmutter, S. 1998b, ApJ, 504, 935
- Riess, A. G., et al. 1999a, AJ, 117, 707
- Riess, A. G., et al. 1999b, AJ, 118, 2675
- Riess, A. G. 2000, PASP, 112, 1284
- Riess, A. G., et al. 2000, ApJ, 536, 62
- Riess, A. G., et al. 2001, ApJ, 560, 49
- Rowan-Robinson, M. 2002, MNRAS, 332, 352
- Savage, B. D., & Mathis, J. S. 1979, ARA&A, 17, 73
- Schlegel, D. J., Finkbeiner, D. P., & Davis, M. 1998, ApJ, 500, 525 (SFD)
- Schmidt, B. P., et al. 1998, ApJ, 507, 46
- Smith, J. A., et al. 2002, AJ, 123, 2121
- Smith, R. C., et al. 2002, BAAS, 34, 4, 1232

Spergel, D. N., et al. 2003, ApJ, submitted.
Stetson, P. B. 1987, PASP, 99, 191
Stetson, P. B., & Harris, W. E. 1988, AJ, 96, 909
Stoughton, C., et al. 2002, AJ, 123, 485
Suntzeff, N. B., et al. 1999, AJ, 117, 1175
Suntzeff, N. B., et al. 2003, in preparation
Tonry, J., et al. 1999, IAU Circ. 7312
Tonry, J. 2003, in preparation
Tsvetkov, D. Yu. 1982, SvAL, 8, 115
Turatto, M., et al. 1996, MNRAS, 281, 1
Turner, M. S., & Riess, A. G. 2002, ApJ, 569, 18
Wells, L. A., et al. 1994, AJ, 108, 2233
Wilson, G., Cowie, L. L., Barger, A. J., & Burke,
D. J. 2002, AJ, 124, 1258